Life Sciences 90 (2012) 657–665

Contents lists available at SciVerse ScienceDirect

Life Sciences

journal homepage: www.elsevier.com/locate/lifescie

Role of CD69 in acute lung injury

Shunsuke Ishizaki [a,*], Yoshitoshi Kasuya [b], Fuminobu Kuroda [a], Kensuke Tanaka [a,b], Junichi Tsuyusaki [a], Keita Yamauchi [a], Hirofumi Matsunaga [b,c], Chiaki Iwamura [d], Toshinori Nakayama [d], Koichiro Tatsumi [a]

[a] Department of Respirology, Graduate School of Medicine, Chiba University, Chiba, Japan
[b] Department of Biochemistry and Molecular Pharmacology, Graduate School of Medicine, Chiba University, Chiba, Japan
[c] UBE Industries Ltd, Ube, Japan
[d] Department of Immunology, Graduate School of Medicine, Chiba University, Chiba, Japan

ARTICLE INFO

Article history:
Received 29 November 2011
Accepted 6 March 2012

Keywords:
Acute lung injury
CD69 antigen
Lipopolysaccharides
Macrophages

ABSTRACT

Aims: CD69 is an early activation marker in lymphocytes and an important signal transmitter in inflammatory processes. However, its role in acute lung injury (ALI) is still unknown. We used a lipopolysaccharide (LPS)-induced mouse model of ALI to study the role of macrophage-surface CD69 in this condition.
Main methods: We investigated bronchoalveolar lavage fluid (BALF) cell subpopulations, myeloperoxidase levels in lung homogenates, lung pathology, and lung oedema in CD69-deficient ($CD69^{-/-}$) mice 24 h after LPS instillation. We also determined cytokine/chemokine expression levels in BALF and macrophage culture supernatant from $CD69^{-/-}$ and wild type (WT) mice. Also, we investigated CD69, keratinocyte-derived chemokine (KC) and macrophage inflammatory protein (MIP)-2 localization in the lungs after LPS administration. Furthermore, we examined the effect of anti-CD69 antibody on LPS-induced cytokine/chemokine release from cultured macrophages.
Key findings: Our study shows that intratracheal instillation of LPS-induced neutrophilic infiltration, histopathological changes, myeloperoxidase positivity, and oedema in the lung to a lower degree in $CD69^{-/-}$ mice than in WT mice. The immunoreactivities for CD69, KC and MIP2 were induced in the lung of WT mice instilled with LPS and were predominantly localized to the macrophages. Moreover, the cytokine/chemokine expression profile between the two genotypes of cultured macrophages in response to LPS was similar to that observed in the BALF. In addition, anti-CD69 antibody inhibited the LPS-induced cytokine/chemokine expression.
Significance: These results suggest that CD69 on macrophages plays a crucial role in the progression of LPS-induced ALI and may be a potentially useful target in the therapy for ALI.

Introduction

Acute lung injury (ALI) is one of the most important causes of severe respiratory failure. The close association between ALI, sepsis, and pneumonia is important from a clinical perspective. Although its pathogenesis remains ill-defined, ALI involves intrapulmonary neutrophil accumulation (Ware and Matthay, 2000).

The membrane component lipopolysaccharide (LPS), has a vital function in Gram-negative bacterial viability. The trimolecular complex of LPS/LPS-binding protein/CD14-stimulated Toll-like receptor (TLR) 4 signalling induces many early response genes, cytokines, and adhesion proteins, leading to neutrophilic inflammation (Goodman et al., 2003; Haziot et al., 1996; Hoshino et al., 1999). Therefore, a murine model of ALI induced by LPS is used to characterize LPS-induced pulmonary immune responses (Hirano, 1997).

CD69 is a type II transmembrane glycoprotein, a member of the natural killer cell gene complex family of cell surface receptors (Lopez-Cabrera et al., 1993). CD69 is also known as a very early activation marker in human and murine lymphocytes (Cebrian et al., 1988; Marzio et al., 1999). It is constitutively expressed on the surface of platelets and monocytes (Marzio et al., 1999). Moreover, CD69 induction has been shown in activated neutrophils (Gavioli et al., 1992) and macrophages (Marzio et al., 1997) and observed in certain inflammatory diseases (Marzio et al., 1999). Although the specific ligand for CD69 is still undetermined, analysis of CD69-mediated cellular output induced by crosslinking with anti-CD69 monoclonal antibody strongly suggests that it is significant in the biology of hematopoietic cells, and plays a role in T cell activation (Cebrian et al., 1988), platelet aggregation, nitric oxide production by monocytes, and neutrophil degranulation (Gavioli et al., 1992; Marzio et al., 1999). Recent studies in various in vivo models have shown that CD69 plays a critical role in inflammation (Esplugues et

* Corresponding author at: Department of Respirology, Graduate School of Medicine, Chiba University, 1-8-1 Inohana, Chuo-ku, Chiba 260-8670, Japan. Tel.: +81 43 222 7171; fax: +81 43 226 2176.
E-mail address: ishizaki@bj8.so-net.ne.jp (S. Ishizaki).

0024-3205/$ – see front matter © 2012 Elsevier Inc. All rights reserved.
doi:10.1016/j.lfs.2012.03.018

al., 2003; Lamana et al., 2006; Miki-Hosokawa et al., 2009; Murata et al., 2003).

The aim of this study is to investigate whether disruption of the CD69 gene affects LPS-induced ALI. Here, we show that CD69 plays a pivotal role in the pathogenesis of ALI.

Materials and methods

Mice

Male C57BL/6 mice (8–10 weeks old) were purchased from Clea Japan (Tokyo, Japan). $CD69^{-/-}$ mice (C57BL/6 background) were generated as previously described (Murata et al., 2003). All mice were maintained under specific pathogen-free conditions. Animal care was in accordance with the guidelines of Chiba University.

LPS-induced ALI

Mice were anaesthetized with an intraperitoneal injection of tribromoethanol before they received a single 50 μl intratracheal LPS injection (*Escherichia coli* O55:B5, Sigma, St. Louis, MO, USA) in phosphate-buffered saline (PBS) using a Microsprayer (Penn-Century Inc., Wyndmoor, PA, USA) to obtain a dosage of 10 μg LPS/30 g body weight. Control mice received 50 μl PBS alone. After 24 h, mice were anesthetized with pentobarbital and sacrificed.

Collection of bronchoalveolar lavage fluid (BALF)

The trachea was exposed and lavaged 2 times with 1 ml PBS using a 20-gauge catheter. The lavage fluid was centrifuged, and the cell pellet resuspended in PBS for total BALF cell count using a haemocytometer. Diff-Quick staining was then performed to distinguish cell morphology.

Histological and morphometric examination of lungs

The lung tissue was fixed by infusion of 4% paraformaldehyde through the tracheal cannula. The left lung was dissected out and soaked in 4% paraformaldehyde. Paraffin-embedded sections were stained with haematoxylin–eosin.

Myeloperoxidase (MPO) assay

A part of the right lung lobe was homogenized and MPO was quantified using the MPO enzyme-linked immunosorbent assay (ELISA) kit (Hycult Biotechnology, Uden, The Netherlands) according to the manufacturer's instructions. Briefly, 10 mg of the lungs was homogenized in 200 μl lysis buffer as the following composition: 200 mM NaCl, 5 mM EDTA, 10% glycerin, 1 mM PMSF, 1 μg/ml leupeptin, 28 μg/ml aprotinin and Tris–HCl (pH 7.4). Sample aliquots were applied onto microtiter well precoated with capture antibody. After washing, biotinylated tracer antibody was added to each well. After the incubation for binding of biotin to streptavidin-peroxidase conjugate, the color development with tetramethylbenzidine was performed. The color reaction was stopped by the addition of oxalic acid. The absorbance at 450 nm was measured with a spectrophotometer. The mouse MPO concentration of each sample was calculated from the standard curve with various concentrations of mouse MPO by serial dilution.

Wet-to-dry lung weight ratio (W/D)

As an index of lung oedema, the amount of extravascular lung water was calculated. A piece of tissue from the right lung was weighed before and after treatment at 80 °C for 48 h, and wet-to-dry lung weight ratio was calculated.

Western blot array analysis for cytokines/chemokines

The level of cytokines/chemokines in BALF and macrophage culture supernatants was measured by the Mouse Inflammation Antibody Array I (RayBiotech, Norcross, GA, USA) according to the manufacturer's protocol. This assay employs a qualitative western blot (WB) screening technique, which detects 40 cytokines/chemokines.

Measurement of chemokines by ELISA

The quantities of keratinocyte-derived chemokine (KC) and macrophage inflammatory protein (MIP)-2 in the BALF and macrophage culture supernatants were determined by ELISA kits (R&D Systems, Minneapolis, MN, USA) according to the manufacturer's protocols.

Immunohistochemical analysis

The lung fixed in 4% paraformaldehyde/0.1 M sodium phosphate buffer (pH 7.4) was embedded in OCT (SAKURA Finetek, Tokyo, Japan) and cut into 8-μm-thick sections, which were placed on poly-L lysine-coated slides. The sections were stained with a rat monoclonal anti-mouse CD69 antibody (R&D Systems), using the ABC immunohistochemical method, and developed with diaminobenzidine. The sections were then counterstained with haematoxylin. In immunofluorescent study, the sections were pretreated with FcR blocking reagent (Miltenyi Biotec, Auburn, CA, USA), then subjected to double staining with rabbit anti-Iba1 polyclonal antibody (Wako chemicals, Tokyo, Japan) in combination with hamster anti-CD69 monoclonal antibody (abcam, Cambridge, UK), biotinylated anti-KC polyclonal antibody (R&D Systems) or biotinylated anti-MIP-2 polyclonal antibody (R&D Systems) followed by a reaction with Alexa Fluor 488-conjugated anti-rabbit antibody (Invitrogen, Carlsbad, CA, USA), Alexa Fluor 594-conjugated anti-hamster antibody (Invitrogen) or Alexa Fluor 594-conjugated streptavidin (Invitrogen). The sections were simultaneously stained with 4′,6-diamino-2-phenylindole (DAPI). In some experiments, the sections were stained with anti-CD69 antibody in combination with anti-KC antibody or anti-MIP-2 antibody. To confirm the precise localization of Iba1-positive cells, the sections were stained with biotinylated anti-podoplanin/gp36 antibody (Biolegend, San Diego, CA, USA), which detects alveolar epithelial cells and thereby clearly visualizes the alveolar structure.

Primary cultured peritoneal macrophages treated with LPS

Each mouse was anesthetized, and the peritoneal cavity lavaged with ice-cold PBS (5 ml). After centrifugation, the resulting precipitate was suspended in minimum essential medium supplemented with 10% foetal bovine serum. The cells were plated on plastic dishes and incubated for 2 h. Nonadherent cells were then washed out, and the remaining adherent macrophages (over 95% of the adherent cells were Iba1-positive) were further incubated for 24 h. They were then replated at a density of 5×10^5 cells/well on 24-well plates and incubated with or without LPS (100 ng/ml) at 37 °C in a humidified atmosphere (5% CO_2) for 24 h. The culture supernatants were subjected to the western blot array and ELISA. In case of experiments with a neutralizing antibody against CD69 signal (clone H1.2F3), 10 μg/ml anti-CD69 signal antibody or isotype-matched control antibody was applied to the cells prior to the LPS stimulation. The antibody, clone H1.2F3 has been originally identified as an anti-CD69 antibody and thereafter recognized as a neutralizing antibody against CD69 signal with a possibility that it may react with CD69 ligand (Miki-Hosokawa et al., 2009).

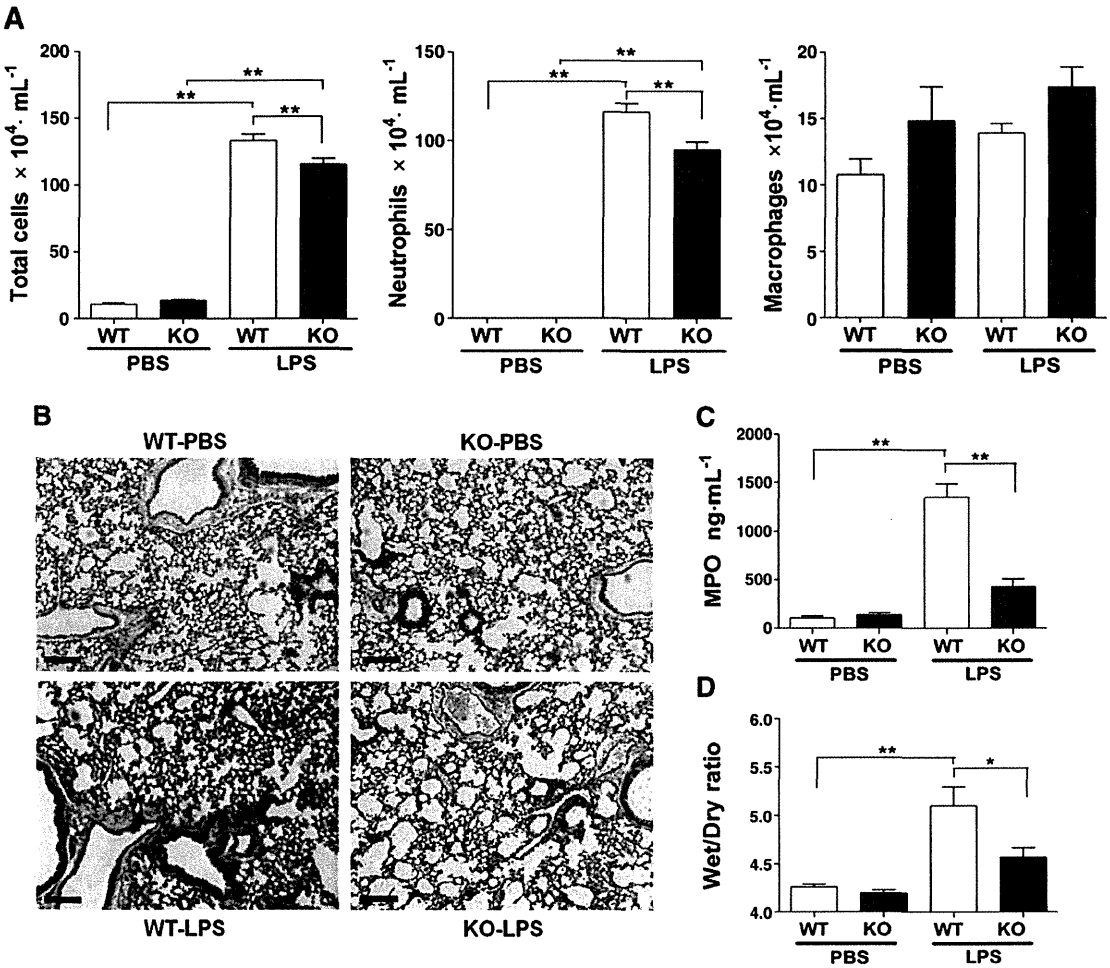

Fig. 1. Involvement of CD69 in LPS-induced neutrophilic inflammation.A) Accumulation of neutrophils in BALF from LPS-challenged mice. LPS (10 μg LPS/30 g body weight) was administered intratracheally to WT and CD69$^{-/-}$ mice. PBS was administered to both genotypes as a control. BALF was collected from mice 24 h after instillation and cell subpopulations determined. Data are shown as mean with SEM (n = 6 per group). $^{**}p<0.01$ (one-way ANOVA, followed by the post-hoc test). B) Effect of CD69 deficiency on histopathological findings in LPS-induced ALI. Histological features of lungs were observed in control- (PBS) and LPS-challenged mice, and the differences between the two genotypes (WT and CD69$^{-/-}$) compared. Mouse lung sections were stained with haematoxylin and eosin. Scale bar = 200 μm. Results were confirmed by similar findings in 3 independent experiments. C) LPS-induced MPO quantification in the lung. Lung homogenates from WT and CD69$^{-/-}$ mice treated with or without LPS were subjected to ELISA for MPO. Data are shown as mean with SEM (n = 6 per group). $^{**}p<0.01$ (one-way ANOVA, followed by the post-hoc test). D) Lung oedema formation induced by LPS. Wet/dry lung weight ratio was measured as an index of lung oedema. Date are shown as mean with SEM (n = 6 per group) $^{*}p<0.05$ (one-way ANOVA, followed by the post-hoc test). LPS: lipopolysaccharide; BALF: bronchoalveolar lavage fluid; WT: wild type; KO: gene-knockout; PBS: phosphate-buffered saline; ALI: acute lung injury; MPO: myeloperoxidase; ELISA: enzyme-linked immunosorbent assay.

Reverse transcription polymerase chain reaction (RT-PCR) detection of LPS signal-related molecules in macrophages

Macrophages from WT and CD69$^{-/-}$ mice in the primary culture were used for RT-PCR to detect TLR-4, myeloid differentiation factor (Myd88), and CD14. Macrophage RNA was isolated using ISOGEN (Wako chemicals) according to the manufacturer's instructions. Single stranded cDNA was synthesized from the prepared RNA (1 μg), with Moloney murine leukemia virus reverse transcriptase (Invitrogen) using an oligo(dT) primer (Invitrogen) in a total volume of 20 μl. The resultant cDNA sample (1 μl) was subjected to PCR for amplification using specific primers. PCR was performed for amplification of mouse TLR-4, Myd88, and CD14 using specific primers (for TLR-4, sense primer, 5′-GCACTGTTCTTCTCCTGCCTG-3′, antisense primer, 5′-AATTGTGAGCCACATTGAGTTTC-3′; for MyD88, sense primer, 5′-TAGAGCTGCTGGCCTTGTTAG-3′, antisense primer, 5′-ATTAGCTCGCTGGCAATGGAC-3′; for CD14, sense primer, 5′-GAGAACACCACCGCTGTAAAG-3′, antisense primer, 5′-AGGGCTCCGAATAGAATCCGAC-3′). The settings of the thermal cycler were 32 cycles of 30 s at 98 °C, 30 s at 54 °C, and 30 s at 72 °C for TLR-4, 32 cycles of 30 s at 98 °C, 30 s at 58 °C, and 30 s at 72 °C for MyD88, 32 cycles of 30 s at 98 °C, 30 s at 58 °C, and 30 s at 72 °C for CD14. We checked the linearity of the reactions to determine the optimal number of cycles for each PCR product. Specific amplification products of the expected size (mouse TLR-4, 438 bp; CD14, 403 bp; MyD88, 368 bp) were observed. As an internal control, the expression of mouse glyceraldehyde-3-phosphate dehydrogenase (GAPDH) was also confirmed.

Statistical analysis

Data are expressed as mean ± SEM. All parameters were evaluated with the Student *t* test or one-way ANOVA, followed by the post-hoc test. A p-value <0.05 was considered significant.

Results

Attenuated LPS-induced neutrophilic inflammation in CD69$^{-/-}$ mice

To determine whether CD69 deficiency affects the LPS-induced infiltration of inflammatory cells into airways and parenchyma, we

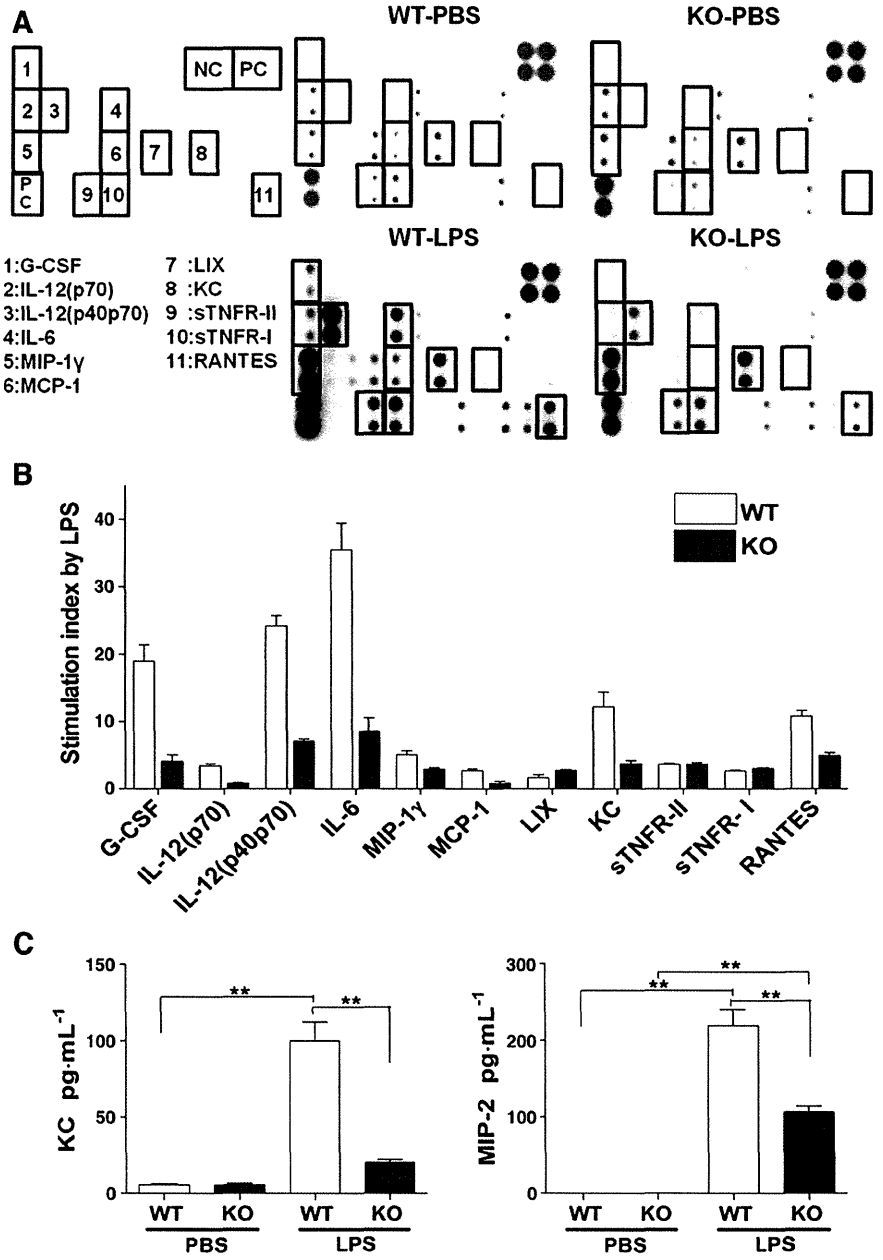

Fig. 2. Changes in cytokine/chemokine expression levels in BALF from the two genotypes after LPS instillation.LPS (10 μg LPS/30 g body weight) or PBS was administered intratracheally to WT and CD69$^{-/-}$ mice. BALF was collected 24 h after instillation and subjected to WB array analysis or ELISA. A) Typical expression profiles of cytokines/chemokines by WB array analysis. The 11 cytokines/chemokines induced by LPS are indicated with the by membrane map location. B) The change in the expression levels of these 11 cytokines/chemokines was analyzed by a densitometer. Each bar is normalized to the individual control signal from PBS-treated mice. Data are shown as mean with SEM (n = 4 per group). C) The concentrations of KC and MIP-2 in BALF were determined by ELISA. Data are shown as mean with SEM (n = 6 per group) $^{**}p<0.01$ (one-way ANOVA, followed by the post-hoc test). BALF: bronchoalveolar lavage fluid; LPS: lipopolysaccharide; PBS: phosphate-buffered saline; WT: wild type; KO: gene-knockout; WB: western blot; ELISA: enzyme-linked immunosorbent assay; KC: keratinocyte-derived chemokine; MIP: macrophage inflammatory protein.

estimated the cell subpopulations in BALF after the LPS administration. LPS induced a stronger inflammatory response characterized by a marked increase in the neutrophil number and total cell count in BALF than that induced by PBS. This induction was significantly greater in WT mice than in CD69$^{-/-}$ mice. On the other hand, there was no difference in macrophage number between the two genotypes after LPS administration (Fig. 1A).

To elucidate the lung pathology associated with LPS-induced accumulation of neutrophils in BALF, we first observed the histopathological features of the lung sections. As shown in Fig. 1B, in the two genotypes of mice, LPS induced the infiltration of neutrophils in the lung and thickening of the alveolar walls. However, the severity of LPS-induced inflammation was more prominent in WT mice than in CD69$^{-/-}$ mice. Next, we assessed the amount of MPO expressed by activated neutrophils in the lung homogenates (Fig. 1C). The MPO concentrations in the samples from the LPS-challenged group were greater than those from the PBS group in both genotypes. The induction of MPO was significantly higher in WT mice than in CD69$^{-/-}$ mice. In accordance with these findings, the induction of lung oedema by LPS was also suppressed in CD69$^{-/-}$ mice compared with WT mice (Fig. 1D).

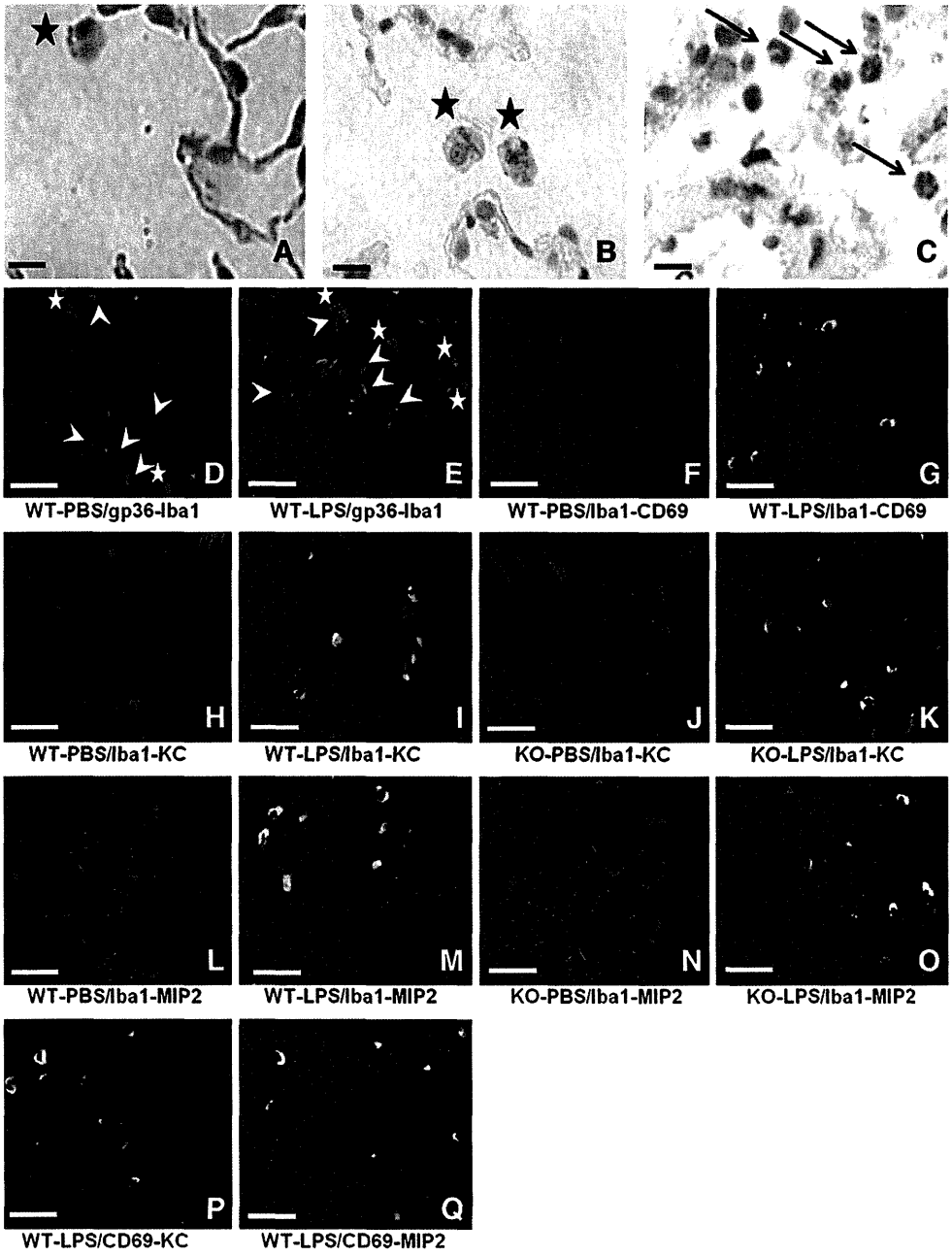

Fig. 3. Immunohistochemical analysis for the localization of CD69, KC and MIP-2 in the lung after LPS instillation.LPS or PBS was administered intratracheally to WT and CD69$^{-/-}$ mice. Mice were sacrificed 24 h after the challenge. The lung sections from WT mice were stained with an anti-CD69 antibody followed by ABC staining method (A, PBS administration; B and C, LPS administration). Asterisks and arrows indicate alveolar macrophages and neutrophils, respectively. The lung sections from WT mice with PBS (D) or LPS administration (E) were stained with anti-Iba1 and biotinylated anti-gp36, followed by a reaction with Alexa Fluor 488-conjugated second antibody and Alexa Fluor 594-conjugated streptavidin, respectively. Each asterisk and arrowhead points to an alveolar macrophage and an interstitial macrophage, respectively. The lung sections from WT mice with PBS (F) or LPS administration (G) were stained with anti-Iba1 and anti-CD69, followed by Alexa Fluor 488-conjugated and Alexa Fluor 594-conjugated second antibodies, respectively. The lung sections from WT (H and I) and CD69$^{-/-}$ mice (J and K) with PBS (H and J) or LPS administration (I and K) were stained with anti-Iba1 and biotinylated anti-KC, followed by Alexa Fluor 488-conjugated second antibody and Alexa Fluor 594-conjugated streptavidin, respectively. The lung sections from WT (L and M) and CD69$^{-/-}$ mice (N and O) with PBS- (L and N) or LPS administration (M and O) were stained with anti-Iba1 and biotinylated anti-MIP-2, followed by Alexa Fluor 488-conjugated second antibody and Alexa Fluor 594-conjugated streptavidin, respectively. The lung sections from WT mice with LPS administration were stained with anti-CD69 in combination with biotinylated anti-KC (P) or biotinylated anti-MIP-2 (Q), followed by Alexa Fluor 594-conjugated second antibody and Alexa Fluor 488-conjugated streptavidin, respectively. All sections were stained with DAPI (D–Q). Each scale bar represents 10 μm (A–C) or 50 μm (D–Q). KC: keratinocyte-derived chemokine; MIP: macrophage inflammatory protein; LPS: lipopolysaccharide; PBS: phosphate-buffered saline; WT: wild type; KO: gene-knockout; DAPI: 4′,6-diamino-2-phenylindole.

Expression of cytokines/chemokines in BALF

We determined the expression level in BALF of cytokines/chemokines that have been reported to be important in recruiting and activating inflammatory cells (Goodman et al., 2003). WB array analysis showed a tendency towards an increase in various cytokine/chemokine levels in BALF from WT mice in the LPS-instilled group compared with those from the PBS group (Fig. 2A). Among these cytokines/chemokines, the induction ratio of granulocyte-colony stimulating factor (G-CSF), interleukin (IL) -12 (p70), IL-12 (p40p70), IL-6, MIP-1γ, monocyte

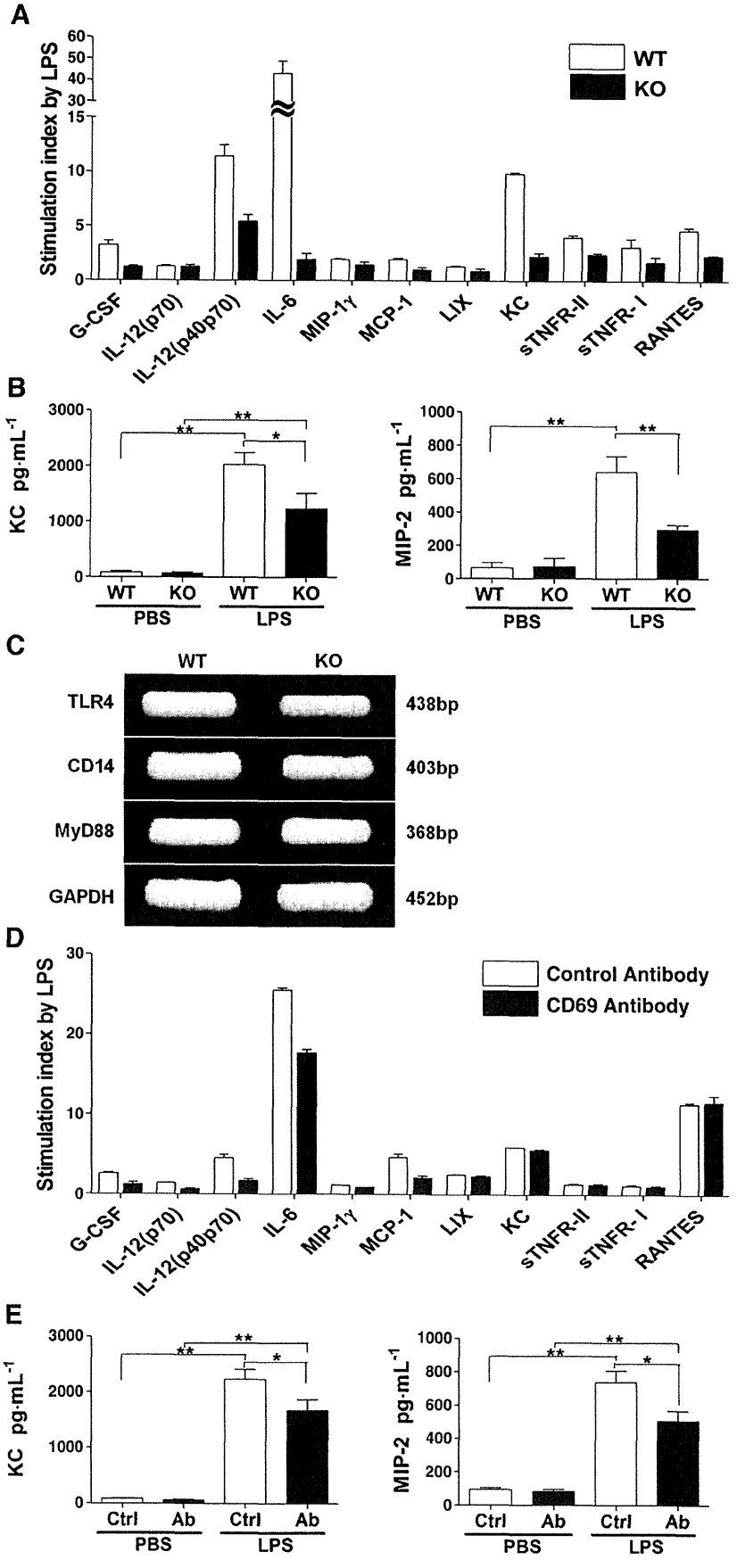
A
Stimulation index by LPS
WT
KO
G-CSF
IL-12(p70)
IL-12(p40p70)
IL-6
MIP-1γ
MCP-1
LIX
KC
sTNFR-II
sTNFR-I
RANTES
B
KC pg·mL-1
MIP-2 pg·mL-1
WT KO WT KO
PBS LPS
C
WT KO
TLR4 438bp
CD14 403bp
MyD88 368bp
GAPDH 452bp
D
Stimulation index by LPS
Control Antibody
CD69 Antibody
E
KC pg·mL-1
MIP-2 pg·mL-1
Ctrl Ab Ctrl Ab
PBS LPS

chemotactic protein (MCP-1), KC and regulated on activation normal T cell expressed and secreted (RANTES) by LPS was reduced in $CD69^{-/-}$ mice compared with WT mice (Fig. 2B).

Chemokines such as lipopolysaccharide-induced CXC chemokine (LIX), KC, and MIP-2 are known to be the murine IL-8 homologues, and play a critical role in neutrophil recruitment (Tateda et al., 2001). Although there was no difference in the LIX induction ratio between the two genotypes, LPS-induced expression of KC was higher in WT mice than in $CD69^{-/-}$ mice (Fig. 2B). MIP-2 was not included in the WB array assay employed in this study. We then performed ELISA to quantify the expression of KC and MIP-2 in BALF. As shown in Fig. 2C, the LPS-induced increase in KC and MIP-2 concentration in BALF from WT mice was significantly higher than in that from $CD69^{-/-}$ mice.

Localization of CD69,KC and MIP-2 in the lung after LPS administration

CD69 has been reported to be induced in activated macrophages and neutrophils (Gavioli et al., 1992; Marzio et al., 1997). Macrophages in the lung of WT mice treated with LPS showed clear CD69-like immunoreactivity (LI), while those in PBS-treated mice did not express CD69. Other cell types including neutrophils showed minimal CD69-LI signal even after LPS administration, indicating that macrophages play a major role in the mechanisms underlying the attenuation of ALI pathology in $CD69^{-/-}$ mice (Fig. 3A–C). To further examine these findings and to evaluate the KC and MIP-2 producing cells, immunofluorescent study was performed. Iba1 recognized alveolar and interstitial macrophages (Fig. 3D and E). A clear CD69-LI was observed predominantly in Iba1-positive macrophages after instillation of LPS (Fig. 3F and G). In addition, LPS-induced KC- and MIP-2-LI in Iba1-positive macrophages in the two genotypes. The number of KC^{+}/$Iba1^{+}$ cells or $MIP\text{-}2^{+}$/$Iba1^{+}$ cells in $CD69^{-/-}$ mice was fewer than that in WT mice (Fig. 3H–O). Furthermore, the localization of KC- and MIP-2-LI was synchronized with that of CD69-LI (Fig. 3P and Q). As the next step, we used cultured macrophages to elucidate whether macrophages can conduct the immune response seen in ALI.

Response of cultured macrophages to LPS

We utilized peritoneal macrophages for the in vitro assay system. Although some papers pointed out functional differences between peritoneal and alveolar macrophages, peritoneal macrophages have been substituted for alveolar macrophages in most cases about LPS-induced mouse model of ALI (Hu et al., 2004; Skwor et al., 2004; Tasaka et al., 2003; Yan et al., 2006; Yang et al., 2011). As shown in Fig. 4A, WB array analysis revealed that various cytokines/chemokines were likely to be induced in the supernatant of cultured macrophages by LPS application. This profile was very similar to that seen in BALF. A densitometric analysis showed that the induction ratio of G-CSF, IL-12 (p40p70), IL-6, MCP-1, KC, and RANTES by LPS was reduced in macrophages from $CD69^{-/-}$ mice compared with those from WT mice. In an analysis by ELISA, the LPS-induced production of KC and MIP-2 in macrophages from $CD69^{-/-}$ mice was significantly lower than in those from WT mice (Fig. 4B). We further investigated the effects of disruption of the CD69 gene on the mRNA expression levels of molecules involved in LPS signal transduction. Gene-knockout studies have revealed that TLR4, CD14, and MyD88 are known as essential molecules in LPS response (Haziot et al., 1996; Hoshino et al., 1999; Kawai et al., 1999). As shown in Fig. 4C, the mRNA levels of TLR4, CD14, and MyD88 in macrophages were mostly similar in WT and $CD69^{-/-}$ mice. Likewise, the LPS-induced cytokine/chemokine expression in macrophages from WT mice was inhibited by a neutralizing antibody against CD69 signal, the profile of which mimicked that observed in the case of macrophages from $CD69^{-/-}$ mice (Fig. 4D and E).

Discussion

We demonstrated that LPS-induced ALI is clearly attenuated in $CD69^{-/-}$ mice by monitoring the following indices: 1) infiltration of neutrophils into air spaces and parenchyma in the lung, 2) detection of MPO, 3) lung oedema, 4) expression levels of cytokines/chemokines in BALF (Figs. 1 and 2). Notably, we also observed a similar cytokine/chemokine expression profile in response to LPS in both lungs and cultured macrophages, which varied with the presence of the CD69 gene (Figs. 2 and 4). Moreover, the expression of CD69 and key chemokines for neutrophil recruitment such as KC and MIP-2 was exclusively localized to macrophages in the lung instilled with LPS (Fig. 3). These facts suggest that induction of CD69 in macrophages is likely to participate in the pathogenesis of LPS-induced ALI.

CD69 is routinely investigated as an early activation antigen for lymphocytes when studying various immune and inflammatory responses (Cebrian et al., 1988). Besides lymphocytes, other hematopoietic cells such as platelets, monocytes, neutrophils, and macrophages have ability to express CD69 under resting or activated states (Gavioli et al., 1992; Marzio et al., 1997, 1999). In addition to its unique expression profile, CD69 may have a receptor-like ability to drive intracellular signalling (Cebrian et al., 1988; Gavioli et al., 1992; Marzio et al., 1999). These reports suggest that CD69 plays a key role in a certain immune reaction systems. In fact, studies with CD69-null mice have shown that CD69 is involved in various immune responses under pathophysiological conditions as a positive or negative regulator of T lymphocytes (Esplugues et al., 2003; Martin et al., 2010; Miki-Hosokawa et al., 2009). With regard to neutrophilic inflammation, however, CD69 deficiency does not abrogate neutrophil recruitment in several acute inflammation models (Lamana et al., 2006). Moreover, the possibility that CD69 regulates the pathogenesis of ALI has never been proven, although a correlation between ALI and CD69 expression was demonstrated from the viewpoint of a diagnostic marker (Schwulst et al., 2008). Thus, this study is the first to reveal an important role for CD69 in the progression of ALI.

Although the pathophysiological mechanisms of ALI are insufficiently understood, histological evaluation of lungs from patients with ALI has indicated the involvement of substantial accumulation of activated neutrophils, diffuse alveolar damage, loss of epithelial integrity, and increased pulmonary oedema in the development of ALI (Ware and Matthay, 2000). Moreover, neutrophils depletion has been shown to

Fig. 4. Effects of the CD69 gene disruption and a neutralizing antibody against CD69 signal on LPS-induced immune response in macrophages.A) Expression of cytokines/chemokines in the macrophages with or without LPS (100 ng/ml) stimulation was detected by WB array analysis. The change in the expression of 11 cytokines/chemokines induced by LPS was analyzed by a densitometer. Each bar is normalized to the individual signal from macrophages without LPS stimulation. Data are shown as mean with SEM (n = 4 per group). B) The concentrations of KC and MIP-2 in macrophage culture supernatants were determined by ELISA. Data are shown as mean with SEM (n = 6 per group). $^{*}p<0.05$, $^{**}p<0.01$ (one-way ANOVA, followed by the post-hoc test). C) The expression of TLR4, CD14, and Myd88 in macrophages. Total RNA was prepared from peritoneal macrophages from WT and $CD69^{-/-}$ mice and subjected to RT-PCR. As a control, RT-PCR was performed for GAPDH. Similar results were observed in 3 independent experiments. D) Inhibitory effect of a neutralizing antibody against CD69 signal on LPS-induced cytokine/chemokine expression in macrophages. Macrophages were stimulated with LPS (100 ng/ml) in the presence or absence of a neutralizing antibody against CD69 signal, and expression of cytokines/chemokines was detected by WB array analysis. The change in expression of LPS-induced 11 cytokines/chemokines was analyzed by a densitometer. Each bar is normalized to the individual signal from macrophages without LPS stimulation. Data are shown as mean with SEM (n = 4 per group). E) Inhibitory effect of a neutralizing antibody against CD69 signal on the LPS-induced production of KC and MIP-2 in macrophages. The concentrations of KC and MIP-2 in macrophage culture supernatants were determined by ELISA. Data are shown as mean with SEM (n = 6 per group). $^{*}p<0.05$, $^{**}p<0.01$ (one-way ANOVA, followed by the post-hoc test). LPS: lipopolysaccharide; PBS: phosphate-buffered saline; WT: wild type; KO: gene-knockout; WB: western blot; KC: keratinocyte-derived chemokine; MIP: macrophage inflammatory protein; ELISA: enzyme-linked immunosorbent assay; TLR: Toll-like receptor; Myd: myeloid differentiation factor; RNA: ribonucleic acid; RT-PCR: reverse-transcription polymerase chain reaction; GAPDH: glyceraldehyde-3-phosphate dehydrogenase; Ctrl: control antibody; Ab: CD69 antibody.

be protective in a model of lung injury (Looney et al., 2006). These findings strongly suggest that neutrophils are prominent cellular mediators in ALI. The priming of neutrophils by cytokines/chemokines is a necessary event for the targeting and sequestration of neutrophils to the lung (Perl et al., 2008). In accordance with this notion, several of the most potent chemoattractants for neutrophils have been studied in BALF from patients with acute respiratory distress syndrome, a more severe form of ALI (Goodman et al., 2003). On this basis, we investigated the induction of proinflammatory cytokines/chemokines in BALF from mice challenged with LPS, which we expected might be closely related to the mechanisms underlying the attenuated neutrophilic inflammation in $CD69^{-/-}$ mice (Fig. 1). As expected, the expression of various cytokines/chemokines, including G-CSF, IL-6, MCP-1, KC and MIP-2 induced by LPS, was reduced in $CD69^{-/-}$ mice compared with WT mice (Fig. 2). Among them, G-CSF, in addition to playing a critical role in neutrophil recruitment along with KC and MIP-2 as the murine IL-8 homologues (Tateda et al., 2001), augments LPS-induced neutrophil recruitment into the lung (Zhang et al., 2001). On the other hand, IL-6 and MCP-1 are thought to be important in the formation of ALI (Goodman et al., 2003). Thus, these cytokines/chemokines may act in concert in neutrophilic inflammation associated with the development of ALI; their expression is positively regulated by CD69 in response to LPS. The proinflammatory cytokines, tumour necrosis factor (TNF)-α, and IL-1β were not detected in the BALF by WB array analysis under our experimental conditions (24 h after LPS instillation), probably because their expression kinetics in response to LPS may be faster than those of other molecules detected in the present study, as demonstrated in previous reports (Rowe et al., 2002). The contribution of TNF-α and IL-1β to LPS-induced airway inflammation, however, is not essential (Moreland et al., 2001), supporting the idea that the expression profile of the CD69-sensitive cytokines/chemokines detected under our experimental conditions is sufficient to explain the attenuation of LPS-induced ALI in $CD69^{-/-}$ mice.

Macrophages are one of primary sources of chemoattractants for neutrophils in the lung. Previous studies in the lungs of macrophage-deficient mice have clearly demonstrated that the absence of mature macrophages attenuates the induction of IL-6, KC, and MIP-2, the degree of neutrophil influx, and lung injury subsequent to septic challenge (Lomas-Neira et al., 2006). Accordingly, the change in cytokine/chemokine expression induced in cultured macrophages by LPS was similar to that in the BALF from mice challenged with LPS. Furthermore, the inhibitory effect of the CD69 gene disruption on induction of cytokines/chemokines by LPS was also consistent between the in vitro and in vivo approaches (Figs. 2 and 4). This finding can be explained by our results, which show that macrophage CD69 was upregulated in parallel with the induction of KC and MIP-2 in the lungs of mice treated with LPS (Fig. 3), and a previous report suggesting that macrophages express CD69 in response to LPS stimulation (Marzio et al., 1997).

The disruption of a certain gene encoding a signalling molecule often influences a change in expression of other genes. This may lead indirectly to phenomenal phenotypic changes in mutant mice under both resting conditions and specific pathophysiological states (Eisener-Dorman et al., 2009). However, in the case of the LPS-mobilizing signal in macrophages, the disruption of CD69 gene must be directly connected with its loss of function because the mRNA levels in macrophages of TLR4, CD14, and MyD88, key molecules of the LPS signal, did not differ between WT and $CD69^{-/-}$ mice (Fig. 4C). Furthermore, the application of a neutralizing antibody against CD69 signal exhibited an inhibitory effect on LPS-induced cytokines/chemokines in cultured macrophages from WT mice, the profile of which was similar to the case of the CD69 gene-disrupting macrophages (Fig. 4 A,B,D and E). Taken together, these results suggest that CD69 induced by LPS in macrophages can play a stimulatory role in the pathogenesis of LPS-induced ALI.

The question that then arises is how CD69 on macrophages regulates the initiation of inflammation in response to LPS. In the in vivo models, a possible scenario is that a putative ligand induced and expressed on the inflamed tissues may mediate the stimulation of CD69 on inflammatory cells (Miki-Hosokawa et al., 2009; Murata et al., 2003). On the other hand, a previous study has proposed that a putative CD69 ligand expressed on macrophages functions as a proinflammatory molecule (McInnes et al., 1997). This notion fits well with the present data from the in vitro study with cultured macrophages. However, the similarity in the profiles of LPS-induced cytokine/chemokine expression between cultured macrophages and the in vivo study suggests that CD69 functions through a common mechanism in both cases. It is of much interest that CD69 forms a complex with and negatively regulates $S1P_1$, a receptor for Sphingosine-1-phosphate (S1P) (Shiow et al., 2006). Previous study showed that the production of S1P in macrophages could be upregulated by LPS (Hammad et al., 2008). Likewise, it is also known that intravenous administration of S1P reduces inflammatory lung injury in a model of LPS-induced ALI (Szczepaniak et al., 2008). Along these lines, the $S1P/S1P_1$ signalling loop may potentially work as a feedback system to prevent LPS-induced inflammatory response-associated tissue injury. CD69 may lock this pathway, and further study would be needed to clarify this point.

Conclusion

We demonstrated that CD69 on macrophages positively participates in the pathogenesis of LPS-induced ALI. This work gives us a new insight into the molecular mechanism of ALI and possibly a therapeutic strategy.

Conflict of interest statement

The authors declare that there are no conflicts of interest.

Acknowledgements

We wish to thank to Dr. Masahiko Hagihara (UBE Industries Ltd, Ube, Japan) for discussion. This work was supported in part by a Grant-in-Aid for Scientific Research from the Ministry of Education, Science, Sports and Culture of Japan ((B), 21390172 to Y.K.) and a grant to the Respiratory Failure Research Group from the Ministry of Health, Labour and Welfare, Japan.

References

Cebrian M, Yague E, Rincon M, Lopez-Botet M, de Landazuri MO, Sanchez-Madrid F. Triggering of T cell proliferation through AIM, an activation inducer molecule expressed on activated human lymphocytes. J Exp Med 1988;168:1621–37.
Eisener-Dorman AF, Lawrence DA, Bolivar VJ. Cautionary insights on knockout mouse studies: the gene or not the gene? Brain Behav Immun 2009;23:318–24.
Esplugues E, Sancho D, Vega-Ramos J, Martinez C, Syrbe U, Hamann A, et al. Enhanced antitumor immunity in mice deficient in CD69. J Exp Med 2003;197:1093–106.
Gavioli R, Risso A, Smilovich D, Baldissarro I, Capra MC, Bargellesi A, et al. CD69 molecule in human neutrophils: its expression and role in signal-transducing mechanisms. Cell Immunol 1992;142:186–96.
Goodman RB, Pugin J, Lee JS, Matthay MA. Cytokine-mediated inflammation in acute lung injury. Cytokine Growth Factor Rev 2003;14:523–35.
Hammad SM, Crellin HG, Wu BX, Melton J, Anelli V, Obeid LM. Dual and distinct roles for sphingosine kinase 1 and sphingosine 1 phosphate in the response to inflammatory stimuli in RAW macrophages. Prostaglandins Other Lipid Mediat 2008;85:107–14.
Haziot A, Ferrero E, Kontgen F, Hijiya N, Yamamoto S, Silver J, et al. Resistance to endotoxin shock and reduced dissemination of gram-negative bacteria in CD14-deficient mice. Immunity 1996;4:407–14.
Hirano S. Quantitative time-course profiles of bronchoalveolar lavage cells following intratracheal instillation of lipopolysaccharide in mice. Ind Health 1997;35:353–8.
Hoshino K, Takeuchi O, Kawai T, Sanjo H, Ogawa T, Takeda Y, et al. Cutting edge: toll-like receptor 4 (TLR4)-deficient mice are hyporesponsive to lipopolysaccharide: evidence for TLR4 as the Lps gene product. J Immunol 1999;162:3749–52.
Hu B, Jennings JH, Sonstein J, Floros J, Todt JC, Polak T, et al. Resident murine alveolar and peritoneal macrophages differ in adhesion of apoptotic thymocytes. Am J Respir Cell Mol Biol 2004;30:687–93.
Kawai T, Adachi O, Ogawa T, Takeda K, Akira S. Unresponsiveness of MyD88-deficient mice to endotoxin. Immunity 1999;11:115–22.
Lamana A, Sancho D, Cruz-Adalia A, del Hoyo GM, Herrera AM, Feria M, et al. The role of CD69 in acute neutrophil-mediated inflammation. Eur J Immunol 2006;36:2632–8.

Lomas-Neira J, Chung CS, Perl M, Gregory S, Biffl W, Ayala A. Role of alveolar macrophage and migrating neutrophils in hemorrhage-induced priming for ALI subsequent to septic challenge. Am J Physiol Lung Cell Mol Physiol 2006;290:L51–8.
Looney MR, Su X, Van Ziffle JA, Lowell CA, Matthay MA. Neutrophils and their Fc gamma receptors are essential in a mouse model of transfusion-related acute lung injury. J Clin Invest 2006;116:1615–23.
Lopez-Cabrera M, Santis AG, Fernandez-Ruiz E, Blacher R, Esch F, Sanchez-Mateos P, et al. Molecular cloning, expression, and chromosomal localization of the human earliest lymphocyte activation antigen AIM/CD69, a new member of the C-type animal lectin superfamily of signal-transmitting receptors. J Exp Med 1993;178:537–47.
Martin P, Gomez M, Lamana A, Cruz-Adalia A, Ramirez-Huesca M, Ursa MA, et al. CD69 association with Jak3/Stat5 proteins regulates Th17 cell differentiation. Mol Cell Biol 2010;30:4877–89.
Marzio R, Jirillo E, Ransijn A, Mauel J, Corradin SB. Expression and function of the early activation antigen CD69 in murine macrophages. J Leukoc Biol 1997;62:349–55.
Marzio R, Mauel J, Betz-Corradin S. CD69 and regulation of the immune function. Immunopharmacol Immunotoxicol 1999;21:565–82.
McInnes IB, Leung BP, Sturrock RD, Field M, Liew FY. Interleukin-15 mediates T cell-dependent regulation of tumor necrosis factor-alpha production in rheumatoid arthritis. Nat Med 1997;3:189–95.
Miki-Hosokawa T, Hasegawa A, Iwamura C, Shinoda K, Tofukuji S, Watanabe Y, et al. CD69 controls the pathogenesis of allergic airway inflammation. J Immunol 2009;183:8203–15.
Moreland JG, Fuhrman RM, Wohlford-Lenane CL, Quinn TJ, Benda E, Pruessner JA, et al. TNF-alpha and IL-1 beta are not essential to the inflammatory response in LPS-induced airway disease. Am J Physiol Lung Cell Mol Physiol 2001;280:L173–80.
Murata K, Inami M, Hasegawa A, Kubo S, Kimura M, Yamashita M, et al. CD69-null mice protected from arthritis induced with anti-type II collagen antibodies. Int Immunol 2003;15:987–92.
Perl M, Lomas-Neira J, Chung CS, Ayala A. Epithelial cell apoptosis and neutrophil recruitment in acute lung injury-a unifying hypothesis? What we have learned from small interfering RNAs. Mol Med 2008;14:465–75.
Rowe SJ, Allen L, Ridger VC, Hellewell PG, Whyte MK. Caspase-1-deficient mice have delayed neutrophil apoptosis and a prolonged inflammatory response to lipopolysaccharide-induced acute lung injury. J Immunol 2002;169:6401–7.
Schwulst SJ, Muenzer JT, Chang KC, Brahmbhatt TS, Coopersmith CM, Hotchkiss RS. Lymphocyte phenotyping to distinguish septic from nonseptic critical illness. J Am Coll Surg 2008;206:335–42.
Shiow LR, Rosen DB, Brdickova N, Xu Y, An J, Lanier LL, et al. CD69 acts downstream of interferon-alpha/beta to inhibit S1P1 and lymphocyte egress from lymphoid organs. Nature 2006;440:540–4.
Skwor TA, Cho H, Cassidy C, Yoshimura T, McMurray DN. Recombinant guinea pig CCL5 (RANTES) differentially modulates cytokine production in alveolar and peritoneal macrophages. J Leukoc Biol 2004;76:1229–39.
Szczepaniak WS, Zhang Y, Hagerty S, Crow MT, Kesari P, Garcia JG, et al. Sphingosine 1-phosphate rescues canine LPS-induced acute lung injury and alters systemic inflammatory cytokine production in vivo. Transl Res 2008;152:213–24.
Tasaka S, Ishizaka A, Yamada W, Shimizu M, Koh H, Hasegawa N, et al. Effect of CD14 blockade on endotoxin-induced acute lung injury in mice. Am J Respir Cell Mol Biol 2003;29:252–8.
Tateda K, Moore TA, Newstead MW, Tsai WC, Zeng X, Deng JC, et al. Chemokine-dependent neutrophil recruitment in a murine model of *Legionella pneumonia*: potential role of neutrophils as immunoregulatory cells. Infect Immun 2001;69:2017–24.
Ware LB, Matthay MA. The acute respiratory distress syndrome. N Engl J Med 2000;342:1334–49.
Yan YJ, Li Y, Lou B, Wu MP. Beneficial effects of ApoA-I on LPS-induced acute lung injury and endotoxemia in mice. Life Sci 2006;79:210–5.
Yang D, Song Y, Wang X, Sun J, Ben Y, An X, et al. Deletion of peroxiredoxin 6 potentiates lipopolysaccharide-induced acute lung injury in mice. Crit Care Med 2011;39:756–64.
Zhang P, Bagby GJ, Kolls JK, Welsh DA, Summer WR, Andresen J, et al. The effects of granulocyte colony-stimulating factor and neutrophil recruitment on the pulmonary chemokine response to intratracheal endotoxin. J Immunol 2001;166:458–65.

Characterization of sarcoma-like cells derived from endarterectomized tissues from patients with CTEPH and establishment of a mouse model of pulmonary artery intimal sarcoma

TAKAYUKI JUJO[1*], SEIICHIRO SAKAO[1*], MASASHI KANTAKE[1], MIKI MARUOKA[3], NOBUHIRO TANABE[1], YASUNORI KASAHARA[1], KATSUSHI KUROSU[1], MASAHISA MASUDA[3], KENICHI HARIGAYA[2] and KOICHIRO TATSUMI[1]

Departments of [1]Respirology and [2]Molecular and Tumor Pathology, Graduate School of Medicine, Chiba University, Chuo-ku, Chiba 260-8670; [3]Chiba Medical Center, National Hospital Organization, Chuo-ku, Chiba 260-8606, Japan

Received February 6, 2012; Accepted April 20, 2012

DOI: 10.3892/ijo.2012.1493

Abstract. In general, intravascular thrombus formation in the pulmonary arteries is considered to be the most common cause of chronic thromboembolic pulmonary hypertension (CTEPH). The current mainstay of therapy for patients with CTEPH is pulmonary endarterectomy (PEA). Recently, the existence of myofibroblast-like cells in endarterectomized tissues has been demonstrated. At the 2nd passage of these myofibroblast-like cells, a pleomorphic cell type was isolated. Pulmonary intimal sarcoma is a very uncommon neoplastic tumor thought to originate from subendothelial-mesenchymal cells of the pulmonary vascular wall. Because these pleomorphic cells were isolated from the pulmonary vascular beds, it is believed that the analysis of these cells may contribute to the understanding of pulmonary intimal sarcoma. We isolated cells from the endarterectomized tissue from patients with CTEPH and identified one type as sarcoma-like cells (SCLs). The SCLs were characterized as hyperproliferative, anchorage-independent, invasive and serum-independent. Moreover, C.B-17/Icr-*scid*/*scid*Jcl mice injected subcutaneously with SCLs developed solid, undifferentiated tumors at the site of injection, and those injected intravenously with SCLs via the tail vein developed tumors which grew along the intimal surface of the pulmonary vessels, thus, demonstrating the high tumorigenic potential of these cells. The behavior of SCLs indicated that these cells may have a vascular cell-like potential which can affiliate them with the intimal surface of the pulmonary artery, and which may be shared with pulmonary intimal sarcoma. A further investigation of this mouse model with SCLs may elucidate the mechanism(s) underlying the development of pulmonary intimal sarcoma.

Correspondence to: Dr Seiichiro Sakao, Department of Respirology (B2), Graduate School of Medicine, Chiba University, 1-8-1 Inohana, Chuo-ku, Chiba 260-8670, Japan
E-mail: sakaos@faculty.chiba-u.jp

*Contributed equally

Key words: pulmonary hypertension, thrombus, embolism, intimal sarcoma

Introduction

In general, pulmonary emboli originating from deep vein thrombosis are thought to have an important role in the development of chronic thromboembolic pulmonary hypertension (CTEPH) (1,2). Organized and incorporated fibrous thrombi promote the complete obliteration of the pulmonary arteries, thus resulting in an increase in pulmonary vascular resistance. Therefore, the current mainstay of therapy for patients with CTEPH is pulmonary endarterectomy (PEA) (3).

Recently, the existence of not only myofibroblast-like cells, but also endothelial-like cells, in the endarterectomized tissues from patients with CTEPH has been demonstrated (4-6). Moreover, our recent study suggested that these myofibroblast-like cells might release substances that promote the endothelial-mesenchymal transition (EnMT) and/or induce EC dysfunction (7). Indeed, there were transitional cells which co-expressed both endothelial (CD31) and SM [α-smooth muscle actin (SMA)] markers in these tissues from patients with CTEPH (7). At the 2nd passage of the myofibroblast-like cells, a pleomorphic cell type that varied in size and shape, and was characterized by a large nucleus, was isolated from the endarterectomized tissues of patients with CTEPH. Because these cells seemed to be hyperproliferative and anti-apoptotic, they were defined as sarcoma-like cells (SCL) (preliminary data). Pulmonary intimal sarcoma is a very uncommon neoplastic tumor of the cardiovascular system, and only about 125 cases have been reported in the literature (8). This tumor is thought to originate from subendothelial-mesenchymal cells of the pulmonary vascular wall (9). Immunohistochemical examinations of intimal sarcoma demonstrated that these tumors undergo endothelial, fibroblastic, or myofibroblastic differentiation (10). Some studies have demonstrated that

intimal sarcomas have positive staining for α-SMA (11), while others have indicated that they are only positive for vimentin, but not for desmin or α-SMA (12). The pathobiology of pulmonary intimal sarcoma remains largely unknown because of its rarity.

Because the SCL were isolated from endarterectomized tissues, i.e., the pulmonary vascular beds, of patients with CTEPH, it was hypothesized that the analysis of these cells may contribute to our understanding of pulmonary intimal sarcoma, which was defined as a neoplasm arising in the tunica intima of the pulmonary arteries. The aim of this study was to investigate the characteristics of SCL *in vivo* and *in vitro*.

Materials and methods

Cell isolation. Endarterectomized tissues from patients with CTEPH were obtained following PEA performed by M.M. at the Chiba Medical Center, Japan. The details of the cell isolation techniques have been described previously (4). The study was approved by the Research Ethics Committee of Chiba University School of Medicine, and written informed consent was given by all subjects.

Cell lines and reagents. Normal human lung fibroblasts (NHLF) and human pulmonary microvascular endothelial cells (HPMVEC) were purchased from Lonza Inc. (Allendale, NJ, USA) and cultured using EGM and fibroblast growth medium (FGM) supplemented with 5% fetal bovine serum (Lonza Inc.). A549 (lung cancer cell line) cells and HT1080 (fibrosarcoma cell line) cells were obtained from Takara Biomedical (Othsu, Shiga, Japan) and cultured in RPMI-1640 medium supplemented with 5% fetal bovine serum (Lonza Inc.). The following Ab were used for the analyses: mouse anti-vimentin (1:200, Dako, Carpinteria, CA, USA), mouse anti-human desmin (1:100, Dako), mouse anti-α-SM-actin (αSMA) (1:1,000, Sigma-Aldrich, St. Louis, MO, USA), mouse anti-human Ki-67 (1:100, BD Biosciences Pharmingen, San Diego, CA, USA), anti-mouse IgG conjugated with Rhodamine dye (1:500, Molecular Probes, Eugene, OR, USA), rabbit anti-von Willebrand factor (factor VIII) (1:1,000, Dako), and an anti-rabbit IgG conjugated with Alexa-488 fluorescent dye (1:500, Molecular Probes). The Bromodeoxyuridine (BrdU) Flow Kit and the BD BioCoat™ FluoroBlok™ Invasion System (24-multiwells) were purchased from BD Biosciences.

Immunofluorescent staining. The cells were fixed in a 1:1 mixture of methanol and acetone and incubated with the primary antibodies, followed by incubation with the secondary antibodies. Additional details about the method used for immunofluorescent staining have been described previously (4).

BrdU-7-amino-actinomycin D binding assay. The BrdU Flow Kit was used to detect the rate of DNA synthesis. The details of this assay technique have been described previously (4).

Colony-forming assay. Six-well flat-bottomed plates with a two-layer soft agar system including a total of $1x10^4$ cells/well in a volume of 1.5 ml/well in the upper layer were adapted for the colony-forming assay. Additional details on the method used for this assay have been described previously (4).

Cell invasion and migration assay. The BD BioCoat FluoroBlok Invasion System (24-multiwell) was used for the cell migration assays. The details of the cell invasion and migration assay techniques have been previously described (4).

Serum starvation. The cells at passage 4 were seeded at $1x10^5$ in 25-cm^2 flasks and were incubated with serum-free medium for the indicated incubation periods. The details of the serum starvation assay techniques have been described previously (4).

Tumorigenicity studies. Adult male C.B-17/Icr-scid/scidJcl (SCID) mice were purchased from a commercial vendor. Tumors were generated by subcutaneous injection of SCL and intravenous tail vein injection of SCL and A549 into SCID mice (n=10 per group, 20±2.5 g) under Nembutal anesthesia (50 mg/ml). At a subcutaneous inoculation concentration of $1x10^6$ cells per mouse, the SCL consistently produced subcutaneous tumors. At an intravenous injection concentration of $2x10^6$ cells per mouse, the SCL and A549 cells consistently produced intravenous and lung tumors. The mice were sacrificed, and the tumors and the organs were quickly isolated and excised on the appropriate days after intravenous injection. After that, they were fixed in 10% formalin for 48 h, and embedded in paraffin. These tissues were sectioned and prepared for the histological analysis. The animal protocol was approved by the Animal Care and Use Committee of Chiba University School of Medicine.

Labeling of SCL with PKH-26. The lipophilic fluorescent PKH dye, PKH-26 (Sigma-Aldrich), was used to label the SCL. The PKH26 dye was diluted at the recommended concentration and mixed with the SLC for 5 min, according to manufacturer's instructions. These cells were injected intravenously via the tail vein of SCID mice and, on day 21, the mice were sacrificed, and their lungs were quickly isolated and excised. The existence of PKH positive SCL with DAPI staining was confirmed under fluorescent microscopy.

PCR array analysis. RT2 Profiler™ PCR Arrays (SABiosciences, Frederick, MD, USA) were used to analyze the expression of a focused panel of genes involved in various biological processes. The 96-well plate extracellular matrix and adhesion molecules PCR array (PAHS-013) which profiles the expression of 84 key genes involved in the formation of the extracellular matrix and adhesion molecules, were selected to detect the differential expression of genes between SCL and A549. Additional details on the method used for this analysis have been described previously (7).

Statistical analysis. The statistical analyses were performed using data from at least three independent experiments. The results are expressed as the means ± SEM. The data were analyzed using Student's t-test, as appropriate. A value of $p<0.05$ was considered to be significant for all tests.

Results

The cellular composition of endarterectomized tissue from CTEPH patients. As shown previously, a few different cell types were isolated from the endarterectomized tissues in each of the 15 patients with CTEPH (4). One of them was determined

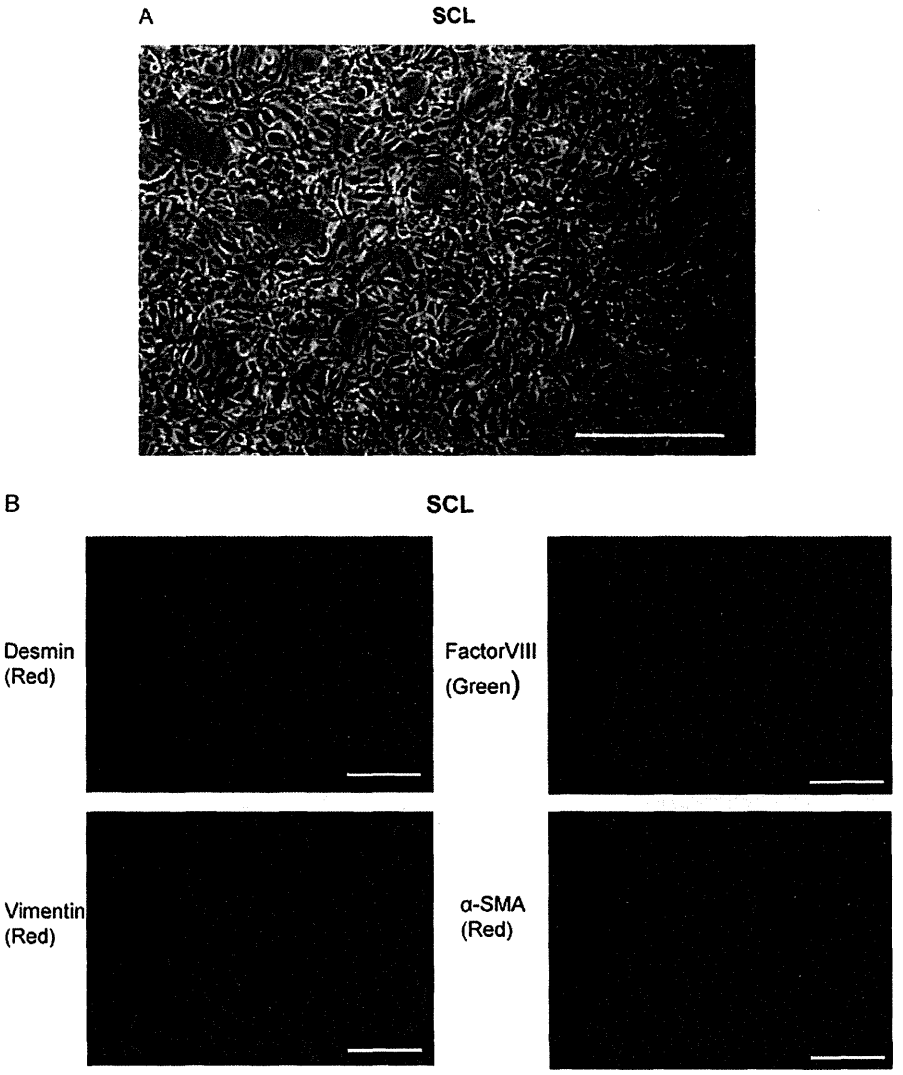

Figure 1. Characterization of the sarcoma-like cells (SCL) from endarterectomized tissue. (A) The SCL from endarterectomized tissue were microscopically assessed. The magnification was x100. Scale bar, 100 μm. (B) SCL derived from endarterectomized tissue were assessed by immunofluorescent staining for desmin, vimentin, factor VIII and α-SMA to confirm the phenotypes of the cells. DAPI staining is shown in blue. The magnification was x200. Scale bar, 50 μm.

morphologically to be the myofibroblast-like cells (spindle-shape with cytoplasmic extensions) (4). At the 2nd passage of the myofibroblast-like cells, another cell type that varied in size and shape and was characterized by a large nucleus, was isolated from one patient described in a previous study (4). These cells had the morphology of SCL (Fig. 1A). The cells outgrown from the thrombotic material were further characterized by immunohistochemical staining for desmin, vimentin, factor VIII and αSMA. The SCL were factor VIII, desmin and αSMA negative, and vimentin positive (Fig. 1B).

Proliferative activity of SCL. The SCL grew without cell-cell contact inhibition and started piling up and forming foci in human fibronectin coated culture dishes (6 cm in diameter) (Fig. 1C). In order to confirm their proliferative activity, the number of proliferating cells which had synthesized DNA was assessed by flow cytometry by immunofluorescent staining of the incorporated BrdU. The number of BrdU positive cells was increased in the SCL, but there was no increase in the incorporation of BrdU by the HPMVEC and NHLF which were used as controls (Fig. 1D).

Anchorage-independent growth of the SCL. Because the growth of the SCL without cell-cell contact inhibition suggested that they would exhibit anchorage-independent growth, we investigated the ability of these cells to form colonies in soft agar. The SCL showed anchorage-independence in the soft agar colony formation assays (Fig. 1E). The colony formation was particularly prominent in the SCL compared with the HPMVEC and NHLF (Fig. 1F).

Invasive and migratory activity of the SCL. Because the SCL exhibited hyperproliferative potential and the ability to undergo anchorage-independent growth, which reflected cancer-related properties (13), we assessed the invasion and migration of the SCL. Using the BD BioCoat FluoroBlok Invasion assay, the SCL, an invasive lung cancer cell line (A549), an invasive fibrosarcoma cell line (HT1080), and the NHLF were allowed to

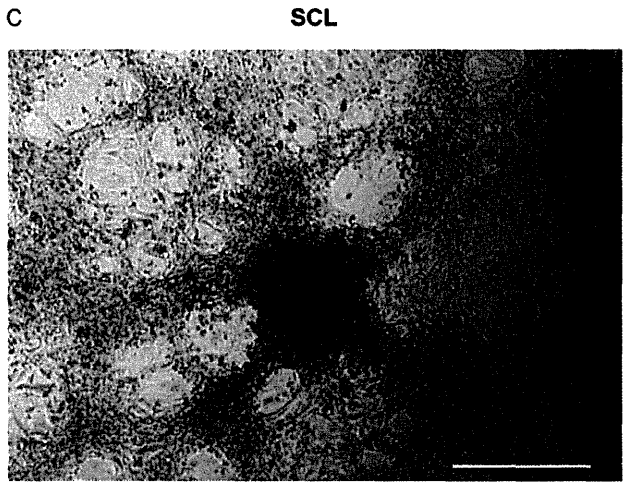

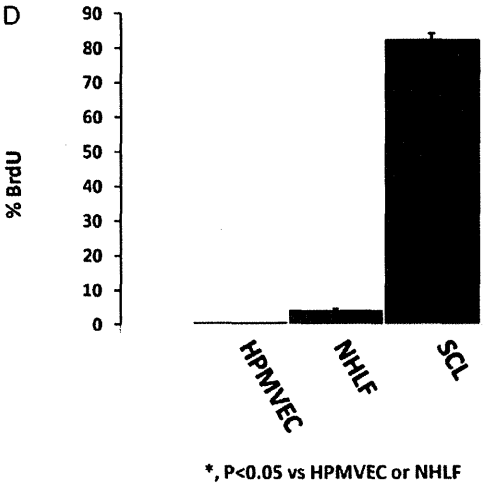

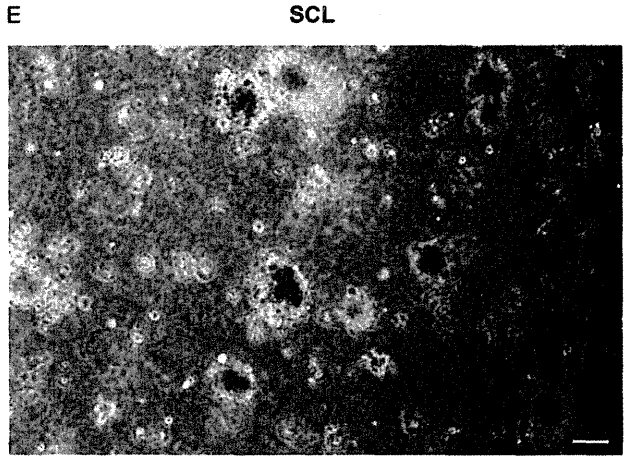

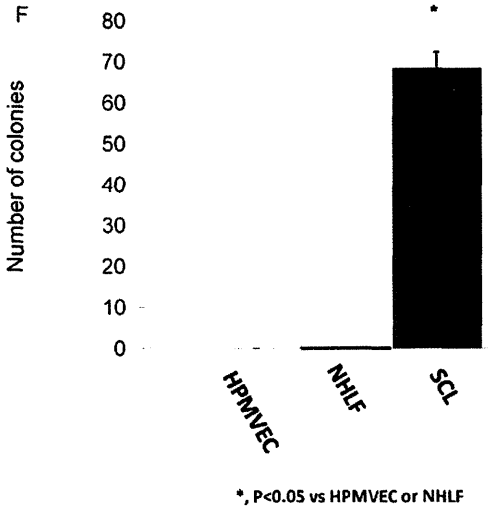

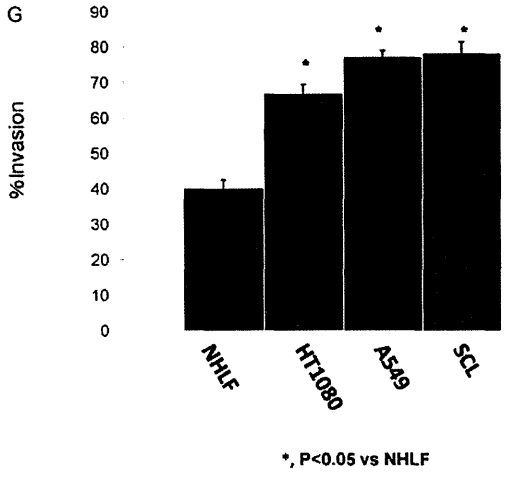

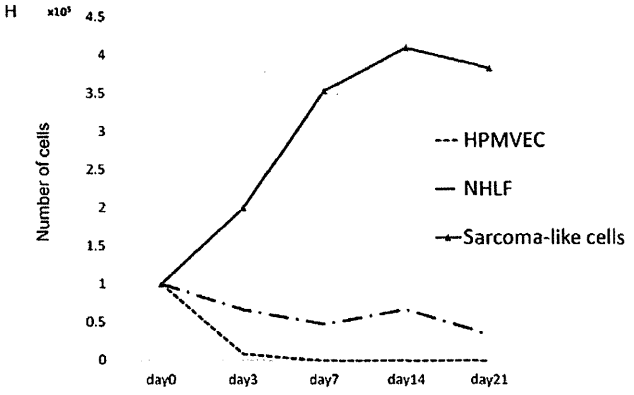

Figure 1. Continued. (C) Light microscopic examination of the SCL at the 3rd passage. The magnification was x100. Scale bar, 100 μm. (D) Quantification of the proliferating SCL at the 4th passage. The individual cells that had synthesized DNA were determined by the immunofluorescent staining of incorporated bromodeoxyuridine (BrdU). The incorporated BrdU was stained with specific anti-BrdU fluorescent antibodies. The levels of cell-associated BrdU were measured by flow cytometry; error bars represent the ± SD from experiments done in triplicate. *p<0.05. (E) The results of the colony-forming assay. SCL at the 4th passage were trypsinized and replated on soft agar. Microphotographs show the colonies grown in soft agar for 2 weeks. The magnification was x40. Scale bar, 100 μm. (F) The numbers of colonies per microscopic field were counted; error bars represent the ± SD from experiments done in triplicate. *p<0.05. (G) The results from the cell invasion and migration assay in SCL. For the BD BioCoat FluoroBlok Invasion assay, NHLF, an invasive fibrosarcoma cell line (HT1080), an invasive lung cancer cell line (A549) and the SCL were allowed to invade for 16 h; error bars represent the ± SD from experiments done in triplicate. *p<0.05. (H) Serum starvation. A comparison of the growth of HPMVEC, NHLF and SCL in the absence of serum. Cells at passage 4 were seeded at $1x10^5$ in 25-cm^2 flasks on day 0 and were incubated with serum-free medium for the indicated incubation periods. On each indicated day, a flask was trypsinized, and the cells counted. The average values of three experiments are shown. SCL, sarcoma-like cells; HPMVEC, human pulmonary microvascular endothelial cells; NHLF, normal human lung fibroblasts.

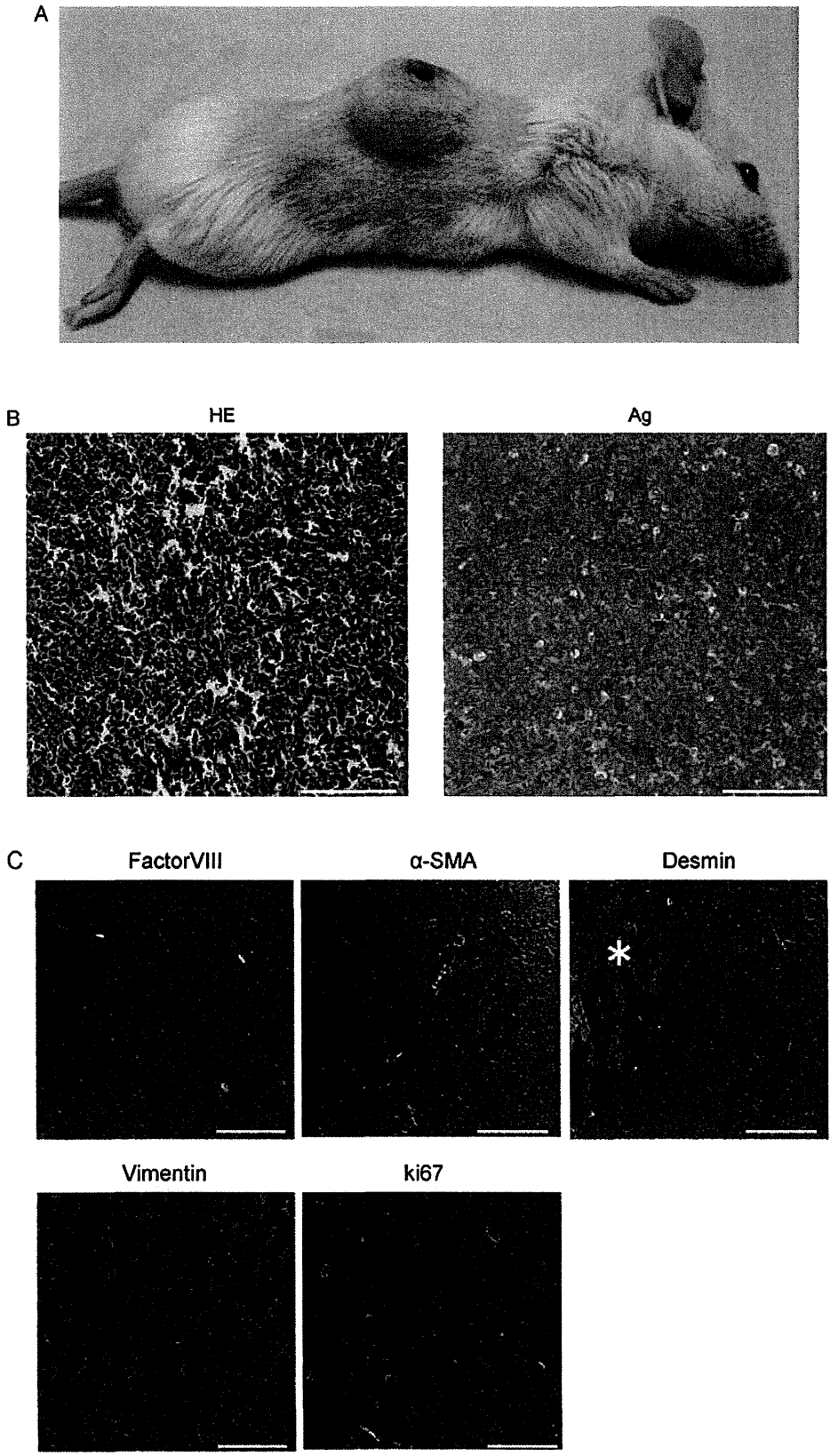

Figure 2. The tumorigenicity of subcutaneously injected SCL. (A) Microphotographs of tumors from a male C.B-17/Icr-scid/scidJcl (SCID) mouse injected subcutaneously with sarcoma-like cells ($1x10^6$ cells per mouse). (B) Hematoxylin/eosin and silver staining of a tumor derived from sarcoma-like cells. Hematoxylin/eosin and silver staining revealed the presence of pleomorphic cells and immature blood vessels (sarcomatous vessels lacking endothelial cells) which favored the escape of tumor metastatic cells and were characterized by reduced collagen production (see Fig. 3B). The magnification was x100. Scale bar, 100 μm. (C) Immunofluorescent staining for factor VIII, αSMA, desmin, vimentin and Ki67 of a tumor derived from sarcoma-like cells. The magnification was x200. Scale bar, 50 μm. *The cells stained positively were smooth muscle cells in a SCID mouse.

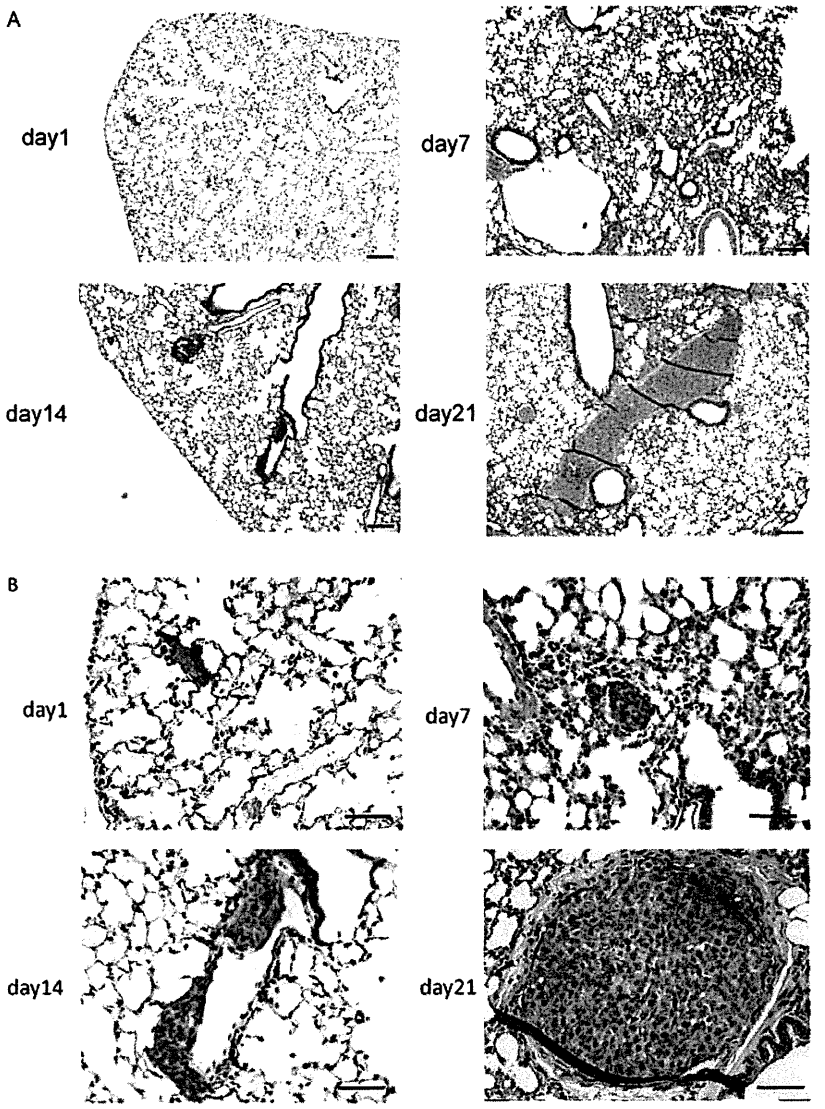

Figure 3. The tumorigenicity of intravenously injected SCL. (A and B) Hematoxylin/eosin staining of lung tumors from a male C.B-17/Icr-scid/scidJcl (SCID) mouse injected intravenously with SCL ($2x10^6$ cells per mouse). Hematoxylin/eosin staining suggested the presence of pleomorphic cells in the pulmonary vessels that increased and migrated in a time-dependent manner. (A) The magnification was x40. Scale bar, 100 μm. (B) The magnification was x100. Scale bar, 50 μm.

invade for 16 h. The SCL showed high invasive and migratory activity, similar to the HT1080 and A549 cells in comparison to the NHLF (Fig. 1G). These findings suggested that the SCL might share an *in vitro* invasive potential with sarcomas and cancer cell lines.

Serum-independent growth of SCL. In the absence of serum, the HPMVEC could not survive, and rapidly underwent apoptosis. Likewise, the NHLF stopped proliferating and gradually died (Fig. 1H). However, the SCL survived indefinitely in the absence of serum and kept proliferating (Fig. 1H).

Subcutaneous tumorigenicity of SCL. In order to test whether these proliferating cells displayed tumorigenic potential, the SCL were injected subcutaneously into SCID mice. Within 4 weeks after s.c. injection (i.e., when tumors had reached a diameter of about 2 cm), 8/8 animals injected with the SCL had developed solid, differentiated tumors at the site of the injection (Fig. 2A), thus demonstrating the high tumorigenic potential of the sarcoma-like cells.

Hematoxylin/eosin (H&E) and silver staining of the sections of a tumor revealed the presence of pleomorphic cells and immature blood vessels (sarcomatous vessels lacking endothelial cells) which favored the escape of tumor metastatic cells and were characterized by reduced collagen production (Fig. 2B). Immunofluorescent staining demonstrated that the cells within the tumors were of mesenchymal origin, neither EC nor SMC, since they were stained negatively for factor VIII, αSMA, and desmin (the cells stained positively were SMC in a SCID mouse) and positively for vimentin (Fig. 2C). The pleomorphic cells were hyperproliferative, as indicated by their expression of the proliferation marker, Ki67 (Fig. 2C).

Tumorigenicity of intravenously injected SCL and A549 cells. In order to test whether the SCL can grow along the intimal surface of the pulmonary artery in a sheet-like form and result in

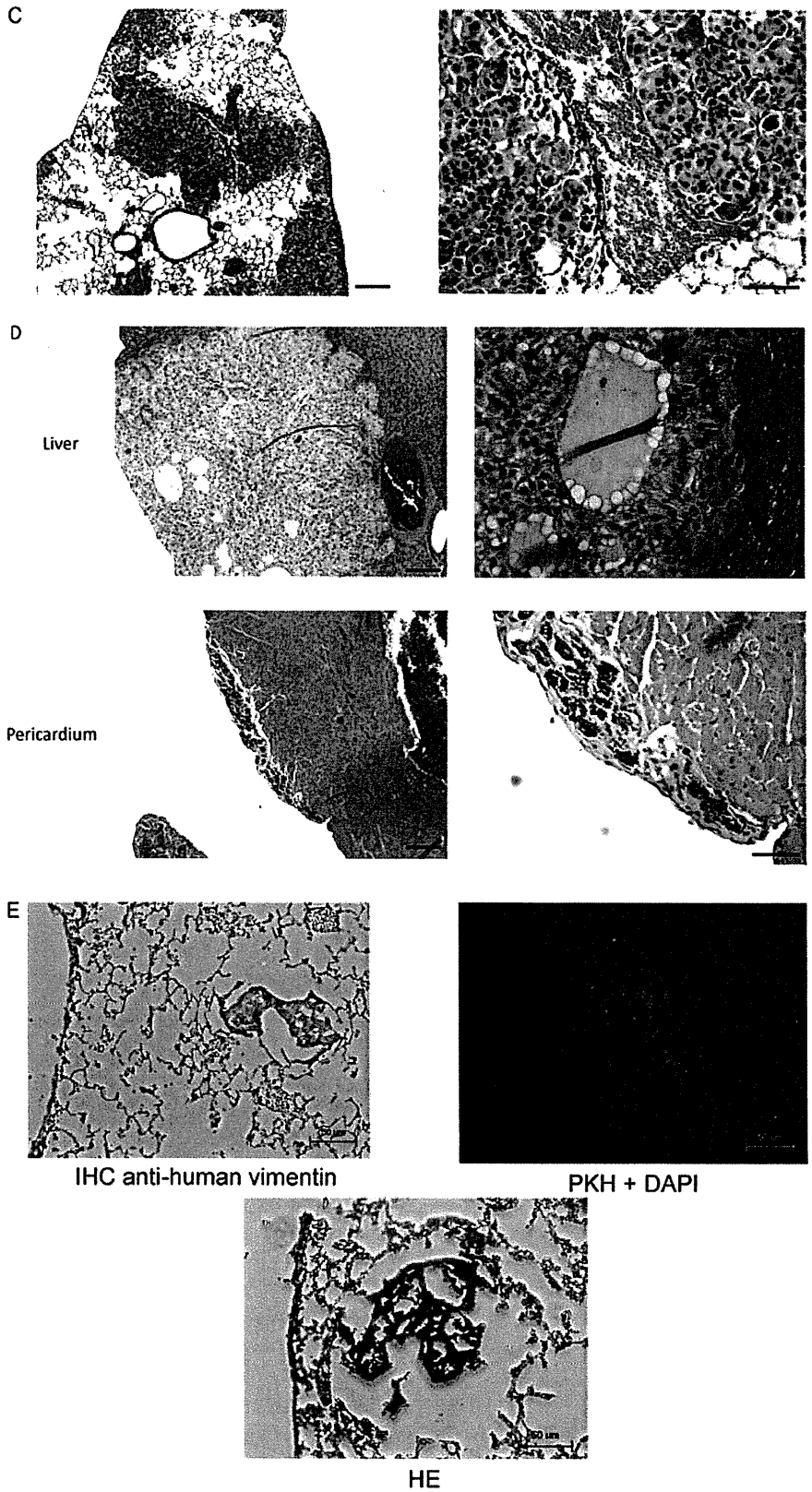

Figure 3. Continued. (C) Hematoxylin/eosin staining of lung tumors from a male C.B-17/Icr-scid/scidJcl (SCID) mouse injected intravenously with A549 cells ($2x10^6$ cells per mouse). Hematoxylin/eosin staining revealed the presence of pleomorphic cells within the lung parenchyma. Left: the magnification was x40, scale bar, 100 μm. Right: the magnification was x100, scale bar, 50 μm. (D) Hematoxylin/eosin staining of the liver and pericardial tumors from a male C.B-17/Icr-scid/scidJcl (SCID) mouse injected intravenously with A549 cells ($2x10^6$ cells per mouse). Hematoxylin/eosin staining revealed the presence of pleomorphic cells in the liver and pericardium. Left: the magnification was x40, scale bar, 100 μm. Right: the magnification was x100, scale bar, 50 μm. (E) Immunohistochemical staining with an anti-human vimentin antibody, double immunofluorescent detection of PKH26 and DAPI, and hematoxylin/eosin staining of lung tumors from a male C.B-17/Icr-scid/scidJcl (SCID) mouse injected intravenously with SCL ($2x10^6$ cells per mouse). These findings indicated that pleomorphic cells originated from the SCL which were injected intravenously via a tail vein. The magnification was x100, scale bar, 50 μm.

Table I. Human extracellular matrix and adhesion molecules PCR array.

Biological process description	Gene name	Gene symbol	Public ID	P-value
Extracellular matrix proteins: collagens & ECM structural constituents	Collagen, type IV, alpha 2	COL4A2	NM_001846	0.049403
Extracellular matrix proteins: collagens & ECM structural constituents	Collagen, type VI, alpha 1	COL6A1	NM_001848	0.003689
Cell adhesion molecules: cell-cell adhesion	Collagen, type VI, alpha 2	COL6A2	NM_001849	0.031248
Extracellular matrix proteins: collagens & ECM structural constituents	Fibronectin 1	FN1	NM_002026	0.005507
Cell adhesion molecules: transmembrane molecules	Integrin, alpha 2 (CD49B, alpha 2 subunit of VLA-2 receptor)	ITGA2	NM_002203	0.004663
Cell adhesion molecules: transmembrane molecules	Integrin, alpha 3 (antigen CD49C, alpha 3 subunit of VLA-3 receptor)	ITGA3	NM_002204	0.037106
Cell adhesion molecules: transmembrane molecules	Integrin, alpha 4 (antigen CD49D, alpha 4 subunit of VLA-4 receptor)	ITGA4	NM_000885	0.005012
Cell adhesion molecules: transmembrane molecules	Integrin, alpha 5 (fibronectin receptor, alpha polypeptide)	ITGA5	NM_002205	0.048419
Extracellular matrix proteins: ECM proteases inhibitors	Kallmann syndrome 1 sequence	KAL1	NM_000216	0.005779
Extracellular matrix proteins: basement membrane constituents	Laminin, alpha 1	LAMA1	NM_005559	0.014549
Extracellular matrix proteins: basement membrane constituents	Laminin, beta 3	LAMB3	NM_000228	0.009781
Cell adhesion molecules: transmembrane molecules	Matrix metallopeptidase 14 (membrane-inserted)	MMP14	NM_004995	0.049414
Extracellular matrix proteins: ECM proteases				
Extracellular matrix proteins: basement membrane constituents	Secreted protein, acidic, cysteine-rich (osteonectin)	SPARC	NM_003118	0.029498
Extracellular matrix proteins: ECM proteases inhibitors	TIMP metallopeptidase inhibitor 2	TIMP2	NM_003255	0.026376
Extracellular matrix proteins: other ECM molecules	Tenascin C	TNC	NM_002160	0.014765

Functional classification of highly expressed genes in SCLs in comparison to A549.

artery occlusion, we investigated the time course of cell growth within the pulmonary artery in comparison to A549 cells.

Hematoxylin/eosin staining of the sections of a lung revealed the presence of pleomorphic cells within the peripheral vessels on day 1, thus suggesting that they were trapped in the pulmonary arteries after intravenous injection [Fig. 3A (small magnification) and B (large magnification)]. The cells spread in a time-dependent manner, and were detected in more distal pulmonary arteries on day 7, grew along the intimal surface of the pulmonary artery in a sheet-like form on day 14, and resulted in artery occlusion on day 21 (Fig. 3A and B). To our surprise, there were no other microscopically visible lesions in any other organs on day 28 after intravenous injection (data not shown).

Hematoxylin/eosin stain demonstrated that there were no pleomorphic cells within the pulmonary vessels on day 21 after intravenous injection of A549 cells. However, these cells developed tumor-like lesions within the lung parenchyma (Fig. 3C). Moreover, there were visible tumor-like lesions within not only the lungs, but also the liver and pericardium (Fig. 3D).

The origin of pleomorphic cells in the pulmonary vessels. To determine the origin of these pleomorphic cells, immunohistochemical staining with an anti-human vimentin antibody and double immunofluorescent detection of PKH26 and DAPI using fluorescence microscopy were performed. The H&E staining of the sections of a lung indicated the presence of pleomorphic cells in the pulmonary vessels (Fig. 3E). These occlusive lesions were composed of some anti-human vimentin positive cells and some PKH26 positive cells (Fig. 3E), thus indicating that these pleomorphic cells could originate from the SCL which were injected intravenously via a tail vein.

The gene expression of extracellular matrix and adhesion molecules by the SCL and A549 cells as determined by a PCR array. The different growth patterns between the SCL and A549 cells

Table II. Human extracellular matrix and adhesion molecules PCR array.

Biological process description	Gene name	Gene symbol	Public ID	P-value
Cell adhesion molecules: other adhesion molecules	Contactin 1	CNTN1	NM_001843	0.004029
Cell adhesion molecules: other adhesion molecules	Collagen, type XII, alpha 1	COL12A1	NM_004370	0.014824
Cell adhesion molecules: cell-cell adhesion	Collagen, type I, alpha 1	COL1A1	NM_000088	0.039601
Cell adhesion molecules: other adhesion molecules	Versican	VCAN	NM_004385	0.014957
Cell adhesion molecules: transmembrane molecules	Integrin, alpha 1	ITGA1	NM_181501	0.015272
Cell-matrix adhesion: cell adhesion molecules	Integrin, alpha 6	ITGA6	NM_000210	0.01777
Transmembrane molecules cell-matrix adhesion				
Extracellular matrix proteins: ECM proteases	Matrix metallopeptidase 7 (matrilysin, uterine)	MMP7	NM_002423	0.002811
Cell adhesion molecules: cell-matrix adhesion	Secreted phosphoprotein 1	SPP1	NM_000582	0.000198
Extracellular matrix proteins: other ECM molecules	Transforming growth factor, beta-induced, 68 kDa	TGFBI	NM_000358	0.003123

Functional classification of low expressed genes in SCLs in comparison to A549.

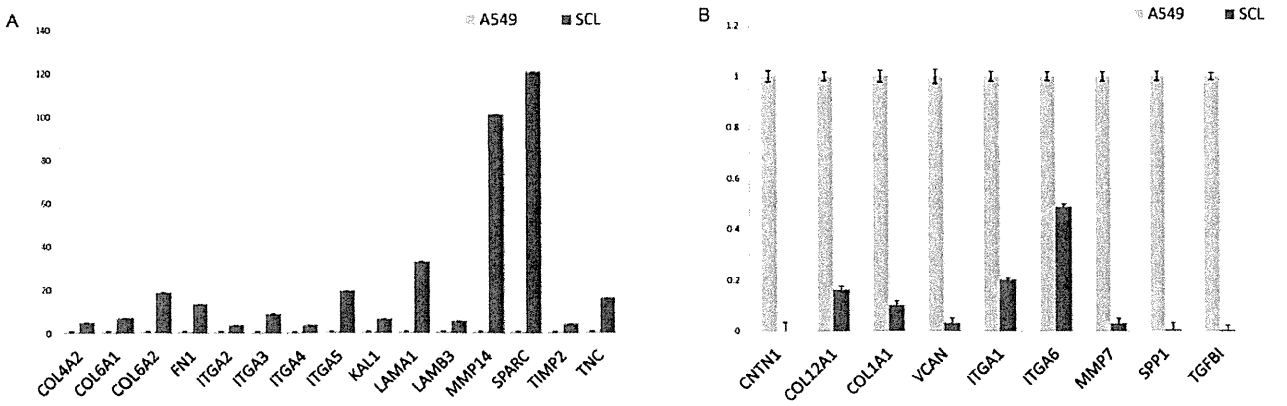

Figure 4. The results of the extracellular matrix and adhesion molecule PCR array. (A) The genes that were more highly expressed in SCL in comparison to A549 cells. There were increases in the expression of 15 extracellular matrix and adhesion molecule-related genes in SCL in comparison to A549 cells ($P<0.05$; n=3). See Table I for definitions of the abbreviations. (B) The genes that were less expressed in the SCL in comparison to A549 cells. There were decreases in the expression of 9 extracellular matrix and adhesion molecule-related genes in the SCL in comparison to the A549 cells ($P<0.05$; n=3). See Table II for definitions of the abbreviations.

after intravenous injection suggested that the cells have different pathophigiological behaviors, which may reflect a difference between epithelial and mescenchymal tumors. Therefore, an extracellular matrix and adhesion molecules PCR array was performed to further characterize the SCL.

The array demonstrated that there were increases in the expression of 15 genes and decreases in the expression of 9 genes in the SCL in comparison to the expression in A549 cells (Fig. 4A and B). The 15 increased genes were COL4A2, COL6A1, COL6A2, FN1, ITGA2, ITGA3, ITGA4, ITGA5, KAL1, LAMA1, LAMB3, MMP14, SPARC, TIMP2, and TNC (Table I).

The 9 genes with an decreased expression were CNTN1, COL12A1, COL1A1, VCAN, ITGA1, ITGA6, MMP7, SPP1, and TGFBI (Table II).

Discussion

In this study, we reported the characterization of cells derived from endarterectomized thrombotic tissues obtained from patients with CTEPH. These cells were defined by their morphology and immunohistochemical staining as SCL (Fig. 1A-C). The SCL were isolated from passaged myofibro-

blast-like cells which had lost their αSMA expression (Fig. 1B) and had morphologically changed from spindle-shaped cells to pleomorphic cells characterized by large nuclei (Fig. 1A). *In vitro*, these SCL displayed anchorage-independent growth and hyperproliferative, invasive and tumorigenic behavior (Fig. 1D-H), raising the question whether pulmonary vessel wall cell transdifferentiation, dedifferentiation, and/or transformation play a role in the development of pulmonary intimal sarcoma.

Angiogenesis, evasion of apoptosis, self-sufficiency in growth signals, insensitivity to anti-growth signals and tissue invasion are considered the features that characterize a malignant cell, and were described in the landmark paper entitled 'Hallmarks of Cancer' by Hanahan and Weinberg (13). We herein demonstrated that SCL from endarterectomized tissue were hyperproliferative (Fig. 1D), anchorage-independent (Fig. 1E and F), invasive (Fig. 1G) and could grow serum-independently (Fig. 1H). All of these traits displayed *in vitro* assays reflect cancer-defining mechanisms, thus suggesting that, as the SCL, intimal sarcoma cells might originate from pluripotent mesenchymal-like cells residing in the conduit vessel endothelium.

The tumorigenic potential of the SCL that were isolated from the myofibroblast-like cells was further demonstrated in SCID mice (Fig. 2A-C). However, these cells were isolated from a single patient. Therefore, it remained unclear whether the *ex vivo* conditions, i.e., factors contained in the culture medium, allowed or induced this transformation or transdifferentiation. Whether there is indeed only one cell type which has the high tumorigenic potential also remains unclear, however, there may be at least two possible sources of the tumorgenic SCL: i) a resident stem-like fibroblast which grows after intimal injury, and ii) a bone marrow-derived precursor cell which migrates to injured arteries during or after thrombus formation.

We reviewed the mechanistic basis of the vascular lesions in PAH, comparing them with each of the cancer-defining mechanisms (13-15). Given this quasi-neoplastic lung vascular cell growth and the cancer-defining mechanisms demonstrated in the cells in this study, it raises the question whether the cells contained in the endarterectomized tissue of the patients with CTEPH possess a latent malignant potential. However, the SCL were isolated from specimens obtained from only one PEA subject, and the SCID mice injected with sarcoma-like cells developed tumors only from the cells isolated from this patient. The conduit vessel endothelium in CTEPH does not exhibit quasi-neoplastic potential, and CTEPH is completely different from neoplastic disease.

Mesenchymal stem cells (MSCs) have the capacity for limitless replicative potential as malignant cells, and could transform themselves from a normal phenotype into a malignant phenotype after *in vitro* passages (16). After intravenous injection of MSCs into the tail veins of mice, these cells could expand rapidly within the lung parenchyma, forming osteosarcoma-like lesions (17). In this study, the bone marrow-derived MSCs which migrate to injured arteries during or after thrombus formation may have developed into the SCL under *in vitro* conditions. However, the SCL could grow along the intimal surface of the pulmonary artery in a sheet-like form and result in the occlusion of the artery (Fig. 3A, B and D), suggesting that the SCL were different from MSCs in terms of their behavior and tumor progression. This indicates that the SCL may themselves have vascular cell-like potential which leads to their affiliation with the intimal surface of the pulmonary artery, and may be shared with pulmonary intimal sarcoma. This is the reason why our investigation into the characteristics of the SCL may elucidate the mechanism of pathogenesis of pulmonary arterial intimal sarcoma.

Although the SCL grew along the intimal surface of the pulmonary artery, the A549 cells expanded rapidly within the lung parenchyma, forming lung cancer-like lesions (Fig. 3C), and resulted in the formation of metastatic lesions in other organs (Fig. 3D). The differences between the mesenchymal cells and epithelial cells may be not sufficient to explain the observed differences between the SCL and A549 cells in tumorigenicity, because MSCs injected intravenously have the potential to develop into tumor-like lesions within the lung parenchyma, similar to A549 cells. Alterations in the expression of extracellular matrix and adhesion molecule genes (Fig. 4A and B) may explain the differences in tumorigenicity between the SCL and A549 cells.

Cell adhesion molecules, including integrins, are receptors located on the cell surface, through which cells can receive important signals from their surroundings, i.e., the basement membrane and extracellular matrix. Laminin is one of the basement membrane proteins, signals from which are transduced through integrin α3β1 to activate the Akt signaling pathway. This activated pathway induces anti-apoptotic effects on these cells (18). The increase in the expression of laminin and integrin α1 genes in the SCL in comparison to A549 cells (Fig. 4A) (Table I) suggests that there was activation of the Akt pathway in the SCL, which may be related to the different cell behaviors between the SCL and A549 cells.

Matrix metalloproteinase (MMP)-7 exhibits proteolytic activity against components of the extracellular matrix (ECM). MMP-7 is frequently overexpressed in invasive cancers of various organs, such as the colon (19), liver (20), lungs (21), and breast (22). Indeed, MMP-7 induces cancer cell invasion under *in vitro* conditions (19,20,23). The observed decrease in the expression of MMP-7 mRNA (Fig. 4B) (Table II) supports our finding that there were no microscopically visible lesions in any other organs after intravenous injection of SCL, although there were metastatic lesions after intravenous injection of A549 cells (Fig. 3D).

This is, to the best of our knowledge, the first description and investigation of cells with *in vitro* and *in vivo* tumorigenic potential that were isolated from the surgically removed thrombotic material of a patient with CTEPH. Whether, and by what mechanism, these cells with a tumorigenic potential contribute to the development of pulmonary intimal sarcoma remains speculative. However, a further investigation of the affinity of SCL for vascular surfaces in this mouse model may elucidate the mechanism underlying the development of pulmonary arterial intimal sarcoma.

Acknowledgements

This study was supported by Research Grants for the Respiratory Failure Research Group and the Cardiovascular Diseases (19-9, 22-33) from the Ministry of Health, Labor and Welfare, Japan, a Grant-in-Aid for Scientific Research (Category C 22590851) from the Japanese Ministry of Education and Science, The Cardiovascular Research Fund, and the Takeda

Science Foundation. K.T. has received honoraria for lectures from Glaxo Smith Kline, Actelion Pharmaceutical Ltd. N.T. has received honoraria for lectures from Actelion, Glaxo Smith Kline, Astellas and Pfizer and research grant support from Actelion Pharmaceutical Ltd. We thank Toshifumi Umemiya in the Department of Molecular and Tumor Pathology, Graduate School of Medicine, Chiba University, for the histological analysis of the mouse tumors.

References

1. Fedullo PF, Kerr KM, AugerWR, Jamieson SW and Kapelanski DP: Chronic thromboembolic pulmonary hypertension. Semin Respir Crit Care Med 21: 563-574, 2000.
2. Moser KM, Daily PO, Peterson K, Dembitsky W, Vapnek JM, Shure D, Utley J and Archibald C: Thromboendarterectomy for chronic, major vessel thromboembolic pulmonary hypertension: immediate and long-term results in 42 patients. Ann Intern Med 107: 560-565, 1987.
3. Jamieson SW, Kapelanski DP, Sakakibara N, Manecke GR, Thistlethwaite PA, Kerr KM, Channick RN, Fedullo PF and Auger WR: Pulmonary endarterectomy: experience and lessons learned in 1,500 cases. Ann Thorac Surg 76: 1457-1464, 2003.
4. Maruoka M, Sakao S, Kantake M, Tanabe N, Kasahara Y, Kurosu K, Takiguchi Y, Masuda M, Yoshino I, Voelkel NF and Tatsumi K: Characterization of myofibroblasts in chronic thromboembolic pulmonary hypertension. Int J Cardiol: Mar 14, 2011 (Epub ahead of print).
5. Yao W, Firth AL, Sacks RS, Ogawa A, Auger WR, Fedullo PF, Madani MM, Lin GY, Sakakibara N, Thistlethwaite PA, Jamieson SW, Rubin LJ and Yuan JX: Identification of putative endothelial progenitor cells ($CD34^+CD133^+Flk\text{-}1^+$) in endarterectomized tissue of patients with chronic thromboembolic pulmonary hypertension. Am J Physiol Lung Cell Mol Physiol 296: L870-L878, 2009.
6. Firth AL, Yao W, Ogawa A, Madani MM, Lin GY and Yuan JX: Multipotent mesenchymal progenitor cells are present in endarterectomized tissues from patients with chronic thromboembolic pulmonary hypertension. Am J Physiol Cell Physiol 298: C1217-C1225, 2010.
7. Sakao S, Hao H, Tanabe N, Kasahara Y, Kurosu K and Tatsumi K: Endothelial-like cells in chronic thromboembolic pulmonary hypertension: crosstalk with myofibroblast-like cells. Respir Res 12: 109, 2011.
8. Bloomberg RD, Butany JW, Cusimano RJ and Leask RL: Primary cardiac sarcoma involving the pulmonary artery and valve. Can J Cardiol 19: 843-847, 2003.
9. Bode-Lesniewska B, Zhao J, Speel EJ, Biraima AM, Turina M, Komminoth P and Heitz PU: Gains of 12q13-14 and overexpression of mdm2 are frequent findings in intimal sarcomas of the pulmonary artery. Virchows Arch 438: 57-65, 2001.
10. Gaumann A, Petrow P, Mentzel T, Mayer E, Dahm M, Otto M, Kirkpatrick CJ and Kriegsmann J: Osteopontin expression in primary sarcomas of the pulmonary artery. Virchows Arch 439: 668-674, 2001.
11. Burke AP and Virmani R: Sarcomas of the great vessels. Cancer 71: 1761-1773, 1993.
12. McGlennen RC, Manivel JC, Stanley SJ, Slater DL, Wick MR and Dehner LP: Pulmonary artery trunk sarcoma: a clinicopathologic, ultrastructural, and immunohistochemical study of four cases. Mod Pathol 2: 486-494, 1989.
13. Hanahan D and Weinberg R: The hallmarks of cancer. Cell 100: 57-70, 2000.
14. Rai PR, Cool CD, King JA, Stevens T, Burns N, Winn RA, Kasper M and Voelkel NF: The cancer paradigm of severe angioproliferative pulmonary hypertension. Am J Respir Crit Care Med 178: 558-564, 2008.
15. Sakao S and Tatsumi K: Vascular remodeling in pulmonary arterial hypertension: multiple cancer-like pathways and possible treatment modalities. Int J Cardiol 147: 4-12, 2011.
16. Loebinger MR, Sage EK and Janes SM: Mesenchymal stem cells as vectors for lung disease. Proc Am Thorac Soc 5: 711-716, 2008.
17. Aguilar S, Nye E, Chan J, Loebinger M, Spencer-Dene B, Fisk N, Stamp G, Bonnet D and Janes SM: Murine but not human mesenchymal stem cells generate osteosarcoma-like lesions in the lung. Stem Cells 25: 1586-1594, 2007.
18. Gu J, Fujibayashi A, Yamada KM and Sekiguchi K: Laminin-10/11 and fibronectin differentially prevent apoptosis induced by serum removal via phosphatidylinositol 3-kinase/Akt- and MEK1/ERK-dependent pathways. J Biol Chem 277: 19922-19928, 2002.
19. Adachi Y, Yamamoto H, Itoh F, Hinoda Y, Okada Y and Imai K: Contribution of matrilysin (MMP-7) to the metastatic pathway of human colorectal cancers. Gut 45: 252-258, 1999.
20. Yamamoto H, Iku S, Adachi Y, Imsumran A, Taniguchi H, Nosho K, Min Y, Horiuchi S, Yoshida M, Itoh F and Imai K: Association of trypsin expression with tumour progression and matrilysin expression in human colorectal cancer. J Pathol 199: 176-184, 2003.
21. Bolon I, Devouassoux M, Robert C, Moro D, Brambilla C and Brambilla E: Expression of urokinase-type plasminogen activator, stromelysin 1, stromelysin 3, and matrilysin genes in lung carcinomas. Am J Pathol 150: 1619-1629, 1997.
22. Heppner KJ, Matrisian LM, Jensen RA and Rodgers WH: Expression of most matrix metalloproteinase family members in breast cancer represents a tumor-induced host response. Am J Pathol 149: 273-282, 1996.
23. Yamamoto H, Adachi Y, Itoh F, Iku S, Matsuno K, Kusano M, Arimura Y, Endo T, Hinoda Y, Hosokawa M and Imai K: Association of matrilysin expression with recurrence and poor prognosis in human esophageal squamous cell carcinoma. Cancer Res 59: 3313-3316, 1999.